

On the Three-Dimensional Structure of Caribbean Mesoscale Eddies

By

Miguel F. Canals Silander

A thesis submitted in partial fulfillment of the requirements for the degree of

MASTER OF MARINE SCIENCE
(Biological Oceanography)

UNIVERSITY OF PUERTO RICO
MAYAGUEZ CAMPUS
2005

Approved by:

Jorge Corredor, Ph.D.
Member, Graduate Committee

Date

Julio Morell, M. Sc.
Member, Graduate Committee

Date

Jose M. Lopez, Ph. D.
President, Graduate Committee

Date

Wilson Ramirez, Ph. D.
Representative of Graduate Studies

Date

Nilda E. Aponte, Ph. D.
Chairperson of the Department

Date

Abstract

The three-dimensional structure of three Caribbean mesoscale features: a cyclone, an anticyclone and an eddy pair, was studied using a combination of in situ and satellite data. The formation and development, hydrography and velocity structure of each feature is studied separately and the results are then compared.

Maximum swirl speeds ranged from 30-60 cm/s and their propagation speeds were 6-12 cm/s. Two of the features, the anticyclone and the eddy pair showed a coherent vertical structure of 1000 meters or more. The vertical structure of the cyclone seemed to be limited to the upper 700 meters of the water column. Thermohaline staircases are found to be more abundant and better defined in the edges of the eddies as compared to their cores.

The formation of these eddies is suggested to be the result of vorticity advected through passages into the Caribbean. Their path into the Caribbean Sea was inferred from SSHA data. The early stages of two of the features entered the Caribbean through the Anegada passage while the third apparently entered through the St. Vincent passage. These features then intensified while they propagated across the Caribbean. It is suggested that the sill depth of the passage through which they enter the Caribbean may be a factor in determining their three-dimensional structure, particularly their vertical extent.

Resumen

Se estudió la estructura tri-dimensional de tres estructuras de meso-escala en el Mar Caribe, un ciclón, un anticiclón y la interacción de un par de remolinos. Se uso una combinación de datos in situ y de satélite. La formación y desarrollo, hidrografía y estructura de corrientes de cada estructura se estudio por separado y luego se compararon entre si.

El rango de velocidades radiales máximas fue 30-60 cm/s y sus velocidades de propagación fueron de 6-12 cm/s. Dos de las estructuras, el anticiclón y el par de remolinos, mostraron una estructura vertical coherente a mas de 1000 metros de profundidad. Sin embargo la estructura vertical del ciclón pareció estar limitada a los primeros 700 metros de la columna de agua. Se encontraron escalones termohalinos dentro de los vortices, los cuales fueron mas abundantes y mas definidos en los bordes de los remolinos que en su centro.

Se sugiere que la formación de las tres estructuras se debió a la advección de vorticidad a través de pasajes hacia el Mar Caribe. Se infirió la ruta de entrada de cada estructura al Caribe usando datos satelitales de anomalía de altura del mar. Las fases tempranas de dos de las estructuras, el anticiclón y el par de remolinos, entraron al Caribe a través del Pasaje de Anegada, mientras que el ciclón entro a través del Pasaje de St. Vincent. Estos remolinos se intensificaron a la vez que se propagaron occidentalmente a través del Caribe. Se sugiere que la profundidad de los pasajes a través del cual entro cada remolino puede ser un factor que afecte su estructura tri-dimensional, especialmente el límite en profundidad de su penetración en la columna de agua.

Acknowledgements

First of all I would like thank my parents Susan Silander and Miguel Canals for their unconditional support throughout my whole life. They have shown me that the only obstacle towards achieving your goals is yourself.

I must also thank my committee: Jose M. Lopez, Jorge Capella, Julio Morell and Jorge Corredor, not only for giving me a job but for introducing me to the world of oceanography. I must also thank them for their friendship, helping me in my research and giving me the opportunity to travel across the Atlantic and Caribbean to conduct oceanographic research. I really appreciate the help obtained from the crews of the RV Chapman and RV Pelican.

I must also thank all my friends from the department for all the good times and all their help: Ramon, Marla, Brandi, Stacey, Katie, Ana, Milton, Alvaro, Alex, Idelfonso and many others. Also thanks to my friends from the west side surfing crew: Ramses, Bebo Arana, Albert Olimpo, Gabriel and many others for all their encouragement. I must also thank all the scientists that have ever lived for giving me the tools to complete this study: from Leibniz and his invention of modern calculus to Joseph Pedlosky's work in Geophysical Fluid Dynamics.

This research was funded by the Office of Naval Research and the National Aeronautic and Space Administration.

Table of Contents

Abstract	ii
Resumen	iii
Acknowledgements	iv
List of Figures	vi
List of tables	viii
List of Appendixes	ix
1. Introduction	1
<i>1.1 Theoretical background</i>	1
<i>1.2 Formation Mechanisms</i>	4
<i>1.3 Importance of mesoscale eddies</i>	5
<i>1.4 Site description</i>	7
2. Objectives	9
3. Previous Studies	10
4. Materials and Methods	13
<i>4.1. Lowered Acoustic Doppler Current Profiler (LADCP):</i>	14
<i>4.2. Conductivity, Temperature and Depth (CTD)</i>	16
<i>4.3. Expendable Bathythermographs</i>	17
<i>4.4. Static stability</i>	17
<i>4.5. Salinity estimation from XBT temperature data</i>	18
<i>4.6. Estimating diapycnal diffusivity</i>	20
<i>4.7 Calculation of geostrophic currents</i>	21
<i>4.8. Satellite altimetry</i>	23
<i>4.9 Nu-Shuttle undulating vehicle</i>	23
5. Results and Discussion	25
5.1 The Cyclone	26
<i>5.1.1 Formation, Development and Motion</i>	28
<i>5.1.2 Hydrography</i>	31
5.2 The anticyclone	36
<i>5.2.1 Formation, development and motion</i>	37
<i>5.2.2 Hydrography</i>	40
<i>5.2.3 Velocity Structure</i>	46
5.3 The cyclone-anticyclone eddy pair	52
<i>5.3.1 Formation, development and motion</i>	54
<i>5.3.2 Hydrography</i>	56
<i>5.3.3 Velocity Structure</i>	60
5.4 Comparing the three features	65
<i>5.4.1 Formation, development and motion</i>	67
<i>5.4.2 Hydrography</i>	69
<i>5.4.3 Velocity structure</i>	73
6. Conclusions	75
7. References	77

List of figures

Figure 1.1 Open and closed streamlines	2
Figure 1.2 A map of The Caribbean Sea shows the main passages between the Atlantic Ocean and the Caribbean (from Johns et al., 2002).....	7
Figure 4.1 LADCP bin setup.....	14
Figure 4.2 Positions of XBT deployments and CTD stations during Cavortex IV.....	19
Figure 4.3 T-S relationship during Cavortex IV. Stommel’s method at 0.1 C intervals compared with the actual data from the 11 CTD stations.....	19
Figure 5.1.1 K490 MODIS image of the cyclonic eddy. Notice the advection of the Orinoco River Plume by the structure.....	26
Figure 5.1.2 AVISO altimetry for August 13, 2003. The arrow indicates the location of the center of the eddy.....	27
Figure 5.1.3 AVISO altimetry shows the apparent formation of the cyclone. (a) An anticyclone collides with the Lesser Antilles and induces a cyclonic circulation on its western side, the cyclonically sheared side. (b) A small cyclone apparently forms as a result of the strengthening of advected vorticity and interacts with adjacent eddies. (c) The cyclone is advected westwards across the Caribbean. By August 13, 2003 the eddy had increased both in size and in amplitude (Figure 5.2.2).	30
Figure 5.1.4 Density (σ_t) structure of the eddy shows shoaling of isopycnals in the top 700 meters of the water column.....	31
Figure 5.1.5 XBT temperature section of the top 200 meters shows shoaling of isotherms indicating upwelling in the center of the eddy.....	32
Figure 5.1.6 Chlorophyll a concentration ($\mu\text{g/L}$) shows an increase of phytoplankton activity in the center of the eddy, around 15 N.....	32
Figure 5.1.7 Meridional section of practical salinity shows a ring of low salinity water around the saltier, oceanic core of the eddy. This is the Orinoco River Plume water being advected by the cyclone as seen in Figure 5.1.1.....	33
Figure 5.1.8 Temperature staircasing at different stations within the eddy. Well defined staircases are missing in the eddy core station.....	34
Figure 5.1.9 Geostrophic velocity along a meridional section across the eddy shows cyclonic rotation with maximum velocities of 40 cm/s. Because the track was N-S, this velocity can be considered as the u-component of the geostrophic flow of the eddy. ..	35
Figure 5.2.1 AVISO merged altimetry for March 12, 2005 showing the area of the study. The arrow indicates the anticyclone that was surveyed.....	36
51	
Figure 5.2.2 AVISO altimetry shows an area of anticyclonic vorticity apparently squeezing into the Caribbean Sea through the Anegada Passage. Arrows show its location at each image taken at two week intervals. This eddy would strengthen considerably by the time it was surveyed in March 2005 southeast of Jamaica.....	37

Figure 5.2.3 AVISO merged altimetry for October 27, 2004 shows the proximity of the anticyclone to Puerto Rico that was eventually surveyed on March 2005 southeast of Jamaica.	38
Figure 5.2.4 LADCP velocity profile on October 22, 2004 at the Caribbean Time Series shows a strong southeast flow in the upper 150 meters. The largest arrow represents a velocity of 37 cm/s. This direction coincides with the direction of the SSHa isolines in Figure 10 suggesting the effects of the eddy were measured at CaTS.	38
Figure 5.2.5 Meridional transect of sigma-t shows the effects of the eddy on the density structure as deep as 1000 meters.	40
Figure 5.2.6 Temperature (in degrees Celsius) distribution at 200 meters from XBT data. Black dots denote XBT drop locations.	41
Figure 5.2.7 Topology of the 22 °C isotherm shows deepening towards the southwest. This presents more evidence that suggests the eddy was indeed merging with another anticyclone during the time period of the survey.	42
Figure 5.2.8 Three-dimensional plot of potential density calculated from the estimated salinity and XBT temperature shows deepening of isopycnals in the meridional and zonal sections. The arrow indicates the cyclonically sheared side of the eddy where density inversions are present.	43
Figure 5.2.9 Zonal section of Nu-Shuttle chlorophyll a fluorescence at the southeastern, cyclonically sheared side of the eddy.	44
Figure 5.2.10 Meridional section at ~74.5 W of Nu-Shuttle chlorophyll a fluorescence along the center of the eddy shows an increase in fluorescence in the edges of the eddy at about 16N and 17.1 N.	44
Figure 5.2.11 Temperature staircasing in different zones within the eddy. The staircases are much more defined in the southeastern edge.	45
Figure 5.2.12 Meridional transect of geostrophic velocity along ~74.5 W shows anticyclonic circulation. Positive values indicate a current towards the east.	46
Figure 5.2.13 Meridional transect along 74.3 W of the zonal velocity component in ms^{-1} . The strongest velocities are confined to the upper 200 meters, yet its anticyclonic structure remains coherent well beyond 1000 meters.	47
Figure 5.2.14 Meridional transect along ~74.3 W of the meridional velocity component in ms^{-1} , stations are denoted by black dots.	47
Figure 5.2.15 Average velocity distribution at different layers.	49
Figure 5.2.16 Contour plot of the base 10 logarithm of current shear squared (in s^{-2}). Overlaid on the figure are sigma-t density contours.	50
Figure 5.2.17 Meridional transect of estimated \log_{10} diapycnal diffusivity (in m^2s^{-2}). Overlaid on the figure are sigma-t density contours.	50
Figure 5.2.18 AVISO SSHa (cm) overlaid on LADCP velocity profiles. The largest arrow represents a velocity of 80 cm/s.	
Figure 5.3.1 AVISO altimetry for July 03, 2004 shows the interaction between the cyclonic eddy (C) and a small anticyclonic eddy (AC).	52
Figure 5.3.2 Notation used in the contour plots. Each black dot denotes a station, and the distance from each station to the first (the southernmost) is given.	53
Figure 5.3.3 AVISO SSHa showing the origins of the interacting features. The arrow shows the location of the cyclonic eddy as it entered the Caribbean. The other	

<i>component of the eddy pair, the small anticyclone, is seen to the right of the cyclone. Due to its weak SSHa signal, its origin is less clear.</i>	55
Figure 5.3.4 <i>Density structure of the eddy pair shows shoaling of isopycnals to the left and deepening to the right caused by the cyclone and anticyclone, respectively.</i>	56
Figure 5.3.5 <i>Nu-Shuttle temperature data shows the effects of the eddy in the near surface layer, causing changes in its thermal structure and in mixed layer depth.</i>	58
Figure 5.3.6 <i>Nu-Shuttle salinity data shows displacement of isohalines in the near surface layer.</i>	58
Figure 5.3.7 <i>Temperature staircasing at different stations within the eddy pair. Staircases are more defined at the transition zone between the eddies than at their cores.</i>	59
Figure 5.3.8 <i>Contour plot of calculated geostrophic velocity in cm/s along the cruise track. Positive values indicate a flow into the figure, a northwesterly flow.</i>	60
Figure 5.3.9 <i>Contour plot of the meridional component of velocity from LADCP stations, denoted by black dots.</i>	61
Figure 5.3.10 <i>Quiver plot of the velocity from LADCP profiles.</i>	61
Figure 5.3.11 <i>Contour plot of the base 10 logarithm of LADCP current shear squared (in s^{-2}).</i>	63
Figure 5.3.12 <i>Transect of estimated \log_{10} diapycnal diffusivity (in m^2s^{-2}), black dots denote individual stations. Besides some isolated “hot spots”, there is no evidence to indicate enhanced diffusivity within the structure.</i>	63
Figure 5.3.13 <i>AVISO merged SSHa (cm) overlaid on LADCP velocity profiles. The largest arrow represents a velocity of 55 cm/s.</i>	64
Figure 5.4.1 <i>Approximate trajectories inferred from SSHa plots of the cyclone (A), the anticyclone (B) and the cyclone (C)-anticyclone (D) eddy pair. The black dot marks the approximate position of the eddy at the time of each cruise.</i>	68
Figure 5.4.2 <i>Temperature-Salinity relationship for the three features: the cyclone, the anticyclone and the eddy pair. The data represent all CTD stations from each cruise.</i>	70
Figure 5.4.3 <i>Depth of the 25 & 26 sigma-t isopycnals at maximum displacement compared with the SSHa of each feature at its center.</i>	71

List of Tables

Table 4.1 *Cruise names, dates and stations.* 13
Table 5.1 *Some descriptive characteristics of the features at the time they were surveyed.*
..... 66

List of Appendixes

Appendix I: Symbols and Notation.....80

1. Introduction

The ocean is turbulent at almost all scales. With the exception of some boundary layers, whether you view the ocean through a microscope or from a satellite, turbulent flows dominate. The ocean is full of eddies: unstable, chaotically unpredictable circulations. Some of these eddies are so small they are dominated by viscosity, others are dominated by the rotation of the earth while others are so large they can “feel” the curvature of the Earth. At all scales they play a large role in the transport of heat, momentum and other properties of the ocean. For the present study we will concentrate on a special kind of eddies, those at the mesoscale.

1.1 Theoretical background

Mesoscale eddies are coherent geophysical structures with a spatial scale on the order of tens of kilometers. They are present virtually everywhere in the ocean, and are the oceanic equivalent to hurricanes. We shall define a mesoscale eddy as a coherent, closed circulation whose lifetime is longer than the time it takes for a fluid parcel to undergo one revolution around its center, and that is confined within the previously described spatial scale. By closed circulation we mean the structure must show closed streamlines (*Figure 1.1*). A streamline is a line of constant streamfunction, where the Eulerian streamfunction $\Psi(x, y, t)$ obeys:

$$u = -\frac{\partial \Psi}{\partial y} \quad v = \frac{\partial \Psi}{\partial x} \quad (1.1)$$

Where $\langle \mathbf{u}, \mathbf{v} \rangle$ are the components of the velocity vector in 2 dimensions. Notice the independence of \mathbf{z} in the streamfunction, because we are talking about two dimensional streamlines in the definition of a mesoscale eddy, as if it was viewed from space. We can

also think of a streamline as a line whose tangent is parallel to the instantaneous velocity vector of the fluid at that point.

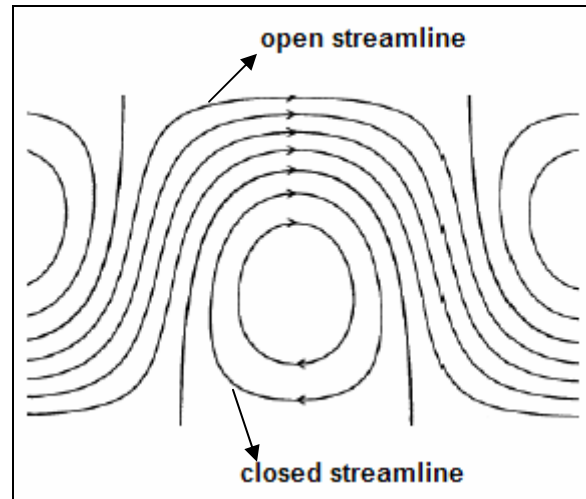


Figure 1.1 Open and closed streamlines

An important property of mesoscale eddies is their vorticity. In the ocean the vorticity due to the currents is called the relative vorticity and is expressed as:

$$\zeta = \nabla \times \mathbf{V} = \frac{\partial v}{\partial x} - \frac{\partial u}{\partial y} \quad (1.2)$$

Where $\mathbf{V} = \langle \mathbf{u}, \mathbf{v} \rangle$ is the velocity vector of the current. Notice that vorticity is in the vertical or \mathbf{z} dimension, and that in the Northern Hemisphere cyclones have positive relative vorticity, while anticyclones have negative relative vorticity. But this vorticity is generated by the eddies' velocity field. There is another type of vorticity, planetary vorticity which itself is responsible for the existence of these mesoscale eddies. It is twice the local rotation of the earth, is denoted by f and is defined as:

$$f = 2\Omega \sin \phi \quad (1.3)$$

Where $\Omega = 7.29 \times 10^{-5}$ is the rotation rate of the earth and Φ is the latitude. The absolute vorticity is $(f + \zeta)$ and is the vorticity “felt” by a parcel of water in the ocean. But a water parcel also “has” a vorticity, which is a conserved property at a large scale. This is the potential vorticity, and its time derivative, where H is the vertical extent of the fluid, is:

$$\frac{D}{Dt} \left(\frac{f + \zeta}{H} \right) = 0 \quad (1.4)$$

.Which means that the quantity:

$$\Pi = \left(\frac{f + \zeta}{H} \right) \quad (1.5)$$

Is conserved following the trajectory of a fluid parcel (see *Cushman-Roisin, 1994* for a derivation). Water parcels in mesoscale eddies conserve their potential vorticity, and this property can be used as a tracer.

Mesoscale eddies are called as such because they tend to equilibrate at a spatial scale of $O(10 \text{ km})$ that varies with latitude and stratification. If it were not for the rotation of the earth and topographic effects, the eddies would keep growing to a larger and larger extent. By the interaction of the pressure gradient and the Coriolis force, eddies tend to stop growing and stabilize at a certain size. This scale is commonly referred to as the internal Rossby radius of deformation, or more simply the length of deformation, L_d , and can be conceptualized as the scale at which rotation and buoyancy effects become equally important. This scale can be quantified as (*Pedlosky, 1979*):

$$L_d = \frac{\sqrt{g'H}}{f} \quad (1.61)$$

Where H is the water depth, f is the Coriolis parameter, and:

$$g' = \frac{\Delta\rho}{\rho_0} g \quad (1.72)$$

Is the reduced gravity felt in the ocean due to very small density differences. Consider a two layer model, with $\Delta\rho = 3 \text{ kg/m}^3$ being the density difference between the layers, $\rho_0 = 1025 \text{ kg/m}^3$ the average density, and $H = 1000 \text{ m}$ as the depth of the two layers.

Substituting these values into equations 1.6 & 1.7 yields a value of $L_d \sim 140 \text{ km}$; similar to the characteristic scale of the eddies visited during the Cavortex expeditions. Note that this scale is undefined at the equator due to the vanishing of the Coriolis force.

1.2 Formation Mechanisms

The subject of the formation of these structures is still an area of active research to this day. Intense Western Boundary Currents (WBC's) such as the Kuroshio produce eddies via the instabilities caused by the meandering of the current. Topographic effects play a large role as would be expected, due to the mechanisms of topographic steering and blocking, caused by the conservation of potential vorticity (*see Cushman-Roisin, 1994, Ch. 4*). Retroflecting currents such as the NBC and the Loop Current (LC) also produce eddies that are pinched off from their retroflexion. These eddies are generally larger than eddies caused by instabilities (*Simmons and Nof, 2001*). Barotropic eddies can be formed by the process of barotropic instability, in which a perturbation of a geophysical flow can exploit a source of energy supplied by the momentum flux due of the meridional shear of the mean flow. Away from boundaries and WBC's, baroclinic instability is the main process for the formation of these eddies (*Gill et al., 1974; Beckman et al., 1994*). The process of baroclinic instability means that a perturbation of a geophysical flow can exploit the energy associated with the vertical shear of the mean

zonal flow (*see Cushman-Roisin, 1994, Ch. 11*). By means of this process, weak oceanic gyres have been shown to generate strong mesoscale eddies (*Spall, 2000*). In the real ocean eddies are frequently generated by mixed barotropic-baroclinic instabilities. Ekman pumping is another process known to generate mesoscale eddies by the slumping of isopycnals (*Oey et al, 2003*), that will in turn create baroclinic instabilities that can grow at the expense of the mean flow.

Once eddies are generated they can be deformed, strained or they can merge in a chaotically unpredictable manner. Once an eddy is in equilibrium, there is a natural tendency for it to keep reaching deeper and deeper in the water column as time goes on. Under ideal conditions, a mesoscale eddy would be able to reach all the way to the bottom of the abysmal ocean, a process known as barotropization. Of course the ocean is far from ideal.

1.3 Importance of mesoscale eddies

Eddies play a principal role in the transfer and interhemispheric exchange of heat, mass and momentum. They modulate the mean flow of the major ocean currents in the World Ocean by exchange of potential energy and momentum. The dynamics of intense WBC's such as the Gulf Stream, the Kuroshio and the North Brazil Current (NBC) are largely determined by mesoscale eddies through the exchange of energy and momentum via instabilities and other processes. Also the kinetic energy of mesoscale variability is much stronger than that of the time-averaged flow (*Gill, 1975*).

The biological importance of mesoscale eddies has also been a subject of intense research. They have been found to trap planktonic communities inside their closed

circulation for as long as a year (*Ring Group, 1981*). *Logerwell and Smith (2001)* found that mesoscale eddies off California increased the survival rate of Pacific sardine larvae. They also play an important role in the isopycnic transport of nutrients (*Lee and Williams, 2000*) which in turn affects the distribution of biological production (*Martin et al., 2002*). Cyclonic eddies produce upwelling that has been observed to locally increase productivity by the upward advection of nutrients into the euphotic zone (*McNeil, 1999*). This process has been called eddy pumping, and has been argued to balance the nutrient budget in the Sargasso Sea (*McGillicuddy and Robinson, 1997; McGillicuddy et al., 1998; Siegel et al., 1999*). Anticyclonic eddies do not create an analogous ecosystem response, as the downwelling they create does not “inhibit” production. So there is an asymmetric biological response in the ocean due to these eddies (*McGillicuddy and Robinson, 1997*). Other eddy-related nutrient pathways to the upper ocean exist, such as ageostrophic circulation that results from perturbation of the circular flow of the eddy (*Martin and Richards, 1999*). This variability caused by mesoscale eddies has been proposed as an explanation to the observed phytoplankton patchiness (*Martin, 2003*). Even the “paradox of the plankton” as proposed by *Hutchinson (1967)*, has been addressed and mesoscale eddies have been suggested as an explanation for the paradox (*Bracco et al., 2000*). Clearly mesoscale eddies have a profound effect on the biology of the ocean.

1.4 Site description

The Caribbean is a semi-enclosed sea bounded by the Greater Antilles to the North, the Lesser Antilles to the East, South America to the South and Central America to the West (*Figure 1.2*).

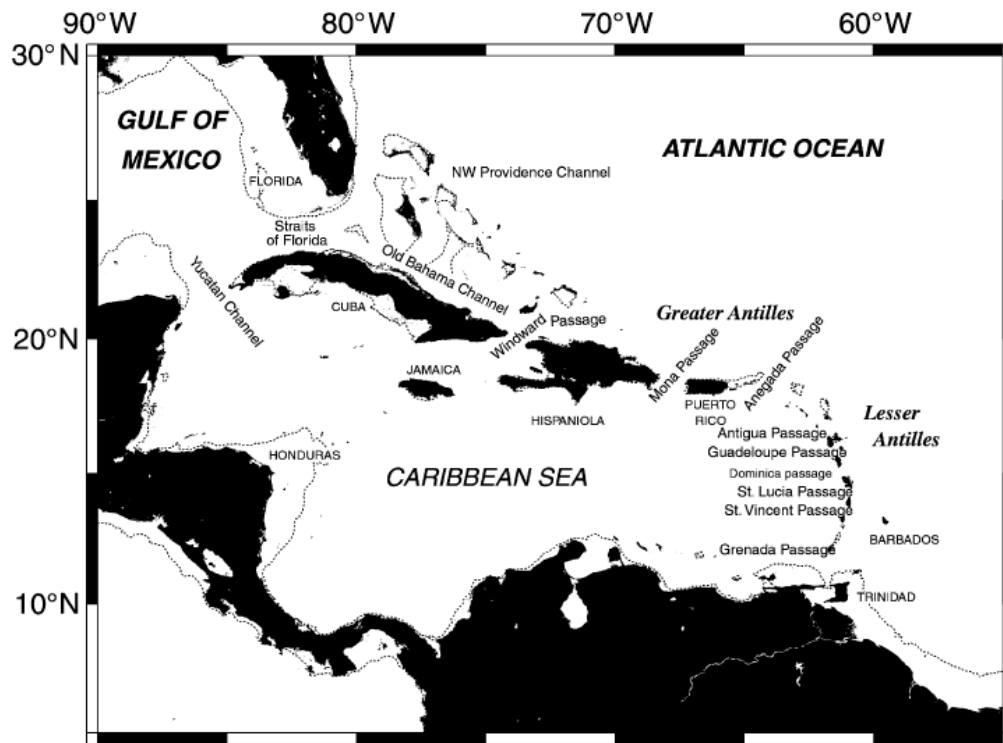


Figure 1.2 A map of The Caribbean Sea shows the main passages between the Atlantic Ocean and the Caribbean (from Johns et al., 2002).

It is the largest marginal sea in the Atlantic Ocean. Its average depth is 4.4 km and is divided into five basins: The Grenada, Venezuela, Colombia, Cayman and Yucatan basins. It comprises the “roots” of the Gulf Stream. A swift mean westward flow called the Caribbean Current (CC) dominates the basin. The CC has been characterized as high speed current ($>25\text{cm/s}$) using drifters by *Richardson (2005)*. Seasonal variability in the strength of the Caribbean current has been reported, with a maximum in July and a minimum in November (*Fuglister, 1951; Johns et al., 2002*). Its path and dynamics are

modulated by the presence of mesoscale and sub-mesoscale eddies, the former being the subject of the present study.

2. Objectives

The main objective of this study is the characterization of the three-dimensional structure of mesoscale eddies in the Caribbean Sea using in situ observations. The emphasis will be on the velocity structure and hydrography of these eddies.

As a final result, the velocity, salinity, thermal and density fields will be analyzed for each feature. Sea Surface Height Anomaly data will be visually analyzed to infer the formation mechanism and movement of the eddies. This data will then be related to the Caribbean Sea eddy variability in general and compared with previous studies of Caribbean eddies.

By no means is this study an unbiased one as the sampling strategy was to, within the logistic time window of a cruise, conduct an expedition to the most notable feature within our reach. One anticyclone, a cyclone and an eddy pair were studied and the obtained data will be used to describe them. However, the structures studied represent the three main types of features that populate the Caribbean Sea eddy field.

The principal hypothesis of this study is that the three-dimensional structure of the eddies will vary depending on their formation mechanism and/or their path into the Caribbean Sea.

3. Previous Studies

Caribbean eddies (CEs) have been studied in detail using satellite altimetry (*Nyusten and Andrade, 1993; Carton and Chao, 1999; Andrade and Barton, 2000; Astor et al., 2003; Goni and Johns, 2003*), numerical modeling (*Heburn et al., 1983; Capella, 1994; Carton and Chao, 1999; Simmons and Nof, 2001; Oey et al., 2003*) and Lagrangian methods such as drogues and floats (*Molinari et al., 1980; Kinder, 1983; Richardson, 2005*). However, Caribbean eddies remain poorly understood because of very few in situ, subsurface observations (*Corredor et al., 2004; Richardson, 2005*).

Numerical simulations have presented evidence for a direct link between the Meridional Overturning Circulation, NBCR's and the eddy variability in the Caribbean Sea (*Murphy et al., 1999; Oey et al., 2003*). They have also been shown to play a large role in the advection of the Orinoco River Plume into the Caribbean Sea (*Corredor et al., 2004*).

The formation of CEs seems to be caused by various processes, and in general is a poorly understood mechanism. It has been hypothesized that the advection of vorticity by North Brazil Current Rings (NBCR's) impinging on the Lesser Antilles might be a cause for the formation of both cyclonic and anticyclonic CEs (*Murphy et al. 1999, Carton and Chao, 1999*). This advected vorticity can act as a finite amplitude perturbation for mixed barotropic and baroclinic instabilities that can amplify or generate mesoscale features in the Caribbean (*Murphy et al., 1999*). The meandering of the Caribbean Current and its associated instabilities has been observed to produce eddies, mainly cyclones to the south and anticyclones to the north of the Current (*Andrade and Barton, 2000*). The wind stress curl has also been implicated in the formation and/or strengthening of CEs, particularly

to the south of Hispaniola (*Andrade and Barton, 2000; Oey et al., 2003*). Using numerical simulations *Oey et al. (2003)* found a patch of anticyclonic wind stress curl south of Hispaniola that can form anticyclones. They found that this wind stress curl can cause a depression of isopycnals by the Ekman pumping mechanism that can produce an anticyclone. This area coincides with high eddy kinetic energy values found by *Richardson (2005)* using drifter data southwest of Hispaniola.

CEs have been observed to propagate westward across the Caribbean Sea at a speed of 10-30 cm/s, with swirl velocities of 20-60 cm/s (*Andrade and Barton, 2000; Murphy et al., 1999; Richardson, 2005*). Their lifetimes have been observed to be around 3-4 months and are modulated by topographic effects and eddy-eddy interactions (*Andrade and Barton, 2000*). Most CEs form in the Eastern Caribbean, and many of these eddies intensify greatly during their generally westward propagation. This intensification has been attributed to different mechanisms, including the wind stress curl (*Andrade and Barton, 2000; Oey et al., 2003*), an inverse energy cascade and the strength of the local currents. Numerical simulations have shown that the degree of intensification depends on the strength of the Caribbean Current, which itself depended on interannual variability in wind forcing (*Murphy et al., 1999*). Seasonal variability in the strength of the Caribbean current has been reported, with a maximum in July and a minimum in November (*Fuglister, 1951; Johns et al., 2002*). This seasonal variability, coupled with the variability of the NBC retroflexion, has been suggested to cause seasonality in Caribbean anticyclone formation (*Richardson, 2005*).

Thermohaline staircases have been observed in a Caribbean cyclonic eddy by *Corredor et al. (2004)* and *Morell et al. (In review)*, particularly in the periphery of the eddy, referred to as the eddy shear zone.

CEs have also been shown by numerical simulations to significantly affect the frequency of eddy shedding by the Loop Current (*Oey et al., 2003*). CEs, particularly strong anticyclones, can induce the shedding of a Loop Current eddy at periods of 14-16 months. Some eddies squeeze through the Yucatan Channel and into the Gulf of Mexico where they can affect the Loop Current and the circulation of the Gulf in general (*Murphy et al., 1999*).

The studies mentioned highlight the importance of CEs in many aspects: advection and turbulent diffusion of river plumes, water mass mixing, modulation of eddy shedding events and their general role in the circulation of the North Atlantic Gyre. What has been lacking, however, are in situ observations of the subsurface structure of these features, especially their velocity structure, hydrography and vertical extent. This is the purpose of the present study.

4. Materials and Methods

As part of the ONR funded project “Characterization of Caribbean Sea mesoscale Eddies”, four cruises were carried out to elucidate the structure of several mesoscale eddies present in the Caribbean Sea. A wealth of scientific instrumentation was used aboard two ships, the R/V Chapman from the University of Puerto Rico and the R/V Pelican from the Louisiana Universities Marine Consortium (LUMCON). Each instrument and the methods used to process the obtained data are explained in detail in the following pages. Following is a summary of the cruises, dates and features studied.

Cruise¹ Name	Feature	Date	Number of full hydrographic stations	Number of LADCP stations	Number of XBT's deployed
Cavortex I	Cyclonic eddy	August 8-15, 2003	7	N/A ²	~20
Cavortex II	Eddy pair	June 21-26, 2004	7	7	~20
Cavortex IV	Anticyclone	March 12-26, 2005	11	11	>100

Table 4.1 Cruise names, dates and stations.

¹ Due to the brevity and limited mesoscale activity, data from the Cavortex III cruise was not used in this study.

² An LADCP was not available during Cavortex I.

4.1. Lowered Acoustic Doppler Current Profiler (LADCP):

The first LADCP cast was made in 1989 at the Hawaii Ocean Time series (HOT) by *Firing and Gordon (1990)*. They suggested the errors might be too large, but when tested by *Fischer and Visbeck (1993)* a year later simultaneously with a Pegasus current profiling device, it was concluded that error could be reduced if care was taken. This instrument has proven itself in WOCE (*Firing, 1998*) and many other expeditions, being very useful due to its capacity of giving full ocean depth profiles.

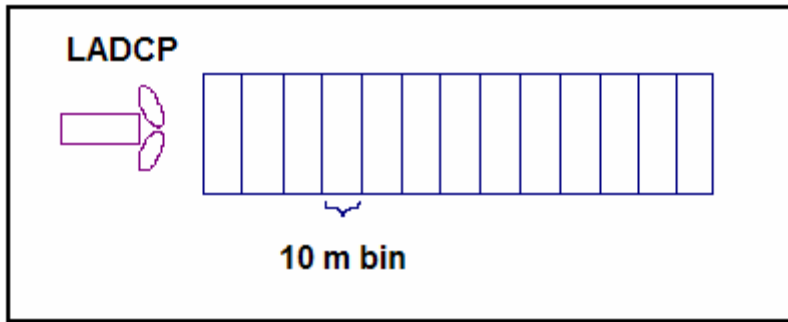


Figure 4.1 LADCP bin setup.

The basic technique of LADCP profiling is the use of overlapping velocity profiles to resolve the full depth velocity field. By itself the LADCP will measure a velocity that contains three components: the motion of the instrument, the velocity of the ocean, and noise:

$$U_{total} = U_{instrument} + U_{ocean} + U_{noise} \quad (4.1)$$

The first of these can be quantified using high accuracy GPS readings, and then integrating:

$$U_{instrument} = \frac{1}{T} \int_0^T U_{ship} dt \quad (4.2)$$

Because the time it takes for the signal to propagate through the water is less than a second, we can assume that $U_{instrument}$ is invariant for each velocity profile. The second component, U_{ocean} , is the velocity profile we are interested in, and is taken to be constant in time. For a typical cast which lasts over an hour, it will be assumed that the profile is constant over that time period, and any variation will be treated as noise, U_{noise} , the third component. In the absence of GPS readings, a baroclinic or depth varying component can be obtained because shear can be calculated over single velocity profiles, based on the assumptions above.

Once the data is obtained it must be processed. First we need to know at what depth the LADCP was when a single profile was measured. There are two ways to do this, and the first is by integrating the vertical velocity measured by the instrument (under the widely accepted assumption based on scaling experiments that vertical velocities in the ocean are very small):

$$z(t) = -\int_0^t w(t)dt \quad (4.3)$$

The other is obviously by using a pressure sensor either on a CTD if mounted on a rosette or on the ADCP itself. We can visualize the ocean velocity profile as the sum of its barotropic and baroclinic components (*Fischer and Visbeck, 1993*):

$$U_{ocean} = U_{ocean,barotropic} + U_{ocean,baroclinic} \quad (4.4)$$

By derivation of the velocity in the vertical dimension we calculate the shear for each profile, and then the shear is averaged for each depth bin, which in our case will be 10 meters. We are now on our way to get the barotropic component. By integrating equation

4.4, then substituting our result into the time integral of equation **4.1** we get (*Fischer and Visbeck, 1993*):

$$\int_0^T U_{ocean,barotropic} dt = \int_0^T U_{total} dt - \int_0^T U_{instrument} dt - \int_0^T U_{ocean,baroclinic} dt - \int_0^T U_{noise} dt \quad (4.5)$$

Using equation **4.2** and assuming the last term of **4.5** is very small yields:

$$U_{barotropic} = \frac{1}{T} \left[\int_0^T U_{instrument} dt - \int_0^T U_{baroclinic}(z) dt \right] - U_{ship} \quad (4.6)$$

Equation **4.6** can be applied to the time series of U_{total} for each 10 m bin (*Fischer and Visbeck, 1993*). The data processing method described above is the one used in Martin Visbeck's LADCP data processing software (version 7.0 beta) written in Matlab code, the one we will use in this study.

This software is available at www.ldeo.columbia.edu/~visbeck/ladcp/. The final results of the processing scheme are the velocity components in Cartesian coordinates for the full depth of the cast.

4.2. Conductivity, Temperature and Depth (CTD)

A Sea Bird SBE-911 CTD was used to obtain conductivity, temperature and pressure values that were used to calculate salinity and depth. From these three quantities, the density, potential density and sigma-t can be calculated using the equation of state of seawater, as well as other derived quantities.

4.3. Expendable Bathythermographs (XBT)

Given the ease of deployment during transit and its affordability, high density XBT sections are ubiquitous in oceanography. These expandable probes allow oceanographers to study the thermal structure of the water column from the surface to its specified maximum range. Two types of probes were used, both manufactured by Sippican, Inc. They were the T-7 probe with a maximum range of 760 meters and maximum deployment velocity of 12 knots, and the T-5 probe with a maximum depth of 1830 meters and a maximum deployment velocity of 5 knots. Each XBT profile used in this study has been carefully subjected to the highest standard of data quality, including accuracy in the geographical position of deployment and visual inspection of each profile for de-spiking purposes.

4.4. Static stability

As a measure of the stratification of the water column, we can define the quantity:

$$N^2 = -\frac{g}{\rho_0} \frac{d\rho}{dz} \quad (4.9)$$

Its square root is the stratification or Brunt-Vaisala frequency, N . This quantity gives us an idea about the frequency of internal waves that the fluid can allow. If $N^2 > 0$ then the fluid is stably stratified, if $N^2 = 0$ the flow is neutral while if $N^2 < 0$ instabilities will arise because there are density inversions. We will use this quantity together with velocity data when calculating gradient Richardson numbers to investigate water column stability inside visited eddies.

4.5. Salinity estimation from XBT temperature data

Given the ease of deployment during transit and its affordability, high density XBT sections are ubiquitous in oceanography. During the Cavortex IV cruise, more than a 100 XBT's were launched to objectively map the thermal structure of a large, coherent anticyclonic eddy in the Caribbean Sea. In addition, 11 CTD stations were occupied across the eddy, and an XBT was launched at each station to compare with the CTD temperature data (*Figure 4.2*). From the CTD data we studied the Temperature-Salinity (TS) curve within the eddy. This TS curve exhibited a tight relationship that can be exploited to estimate salinity from XBT temperature data (*Figure 4.3*).

More than 50 years ago it was noticed that the co-variability of temperature with salinity can be used to estimate salinity (*Stommel, 1947*). An important assumption must be made: that the variability in salinity can be explained by vertical displacements of water parcels with well defined value for temperature and salinity. Given the “tightness” of the TS relationship exhibited during the cruise, we shall make this assumption to estimate salinity from XBT data. Stommel's method uses the mean of the observed salinity on an isothermal surface, independent of pressure:

$$\hat{S} = \langle S \rangle_T \quad (4.10)$$

Where $\langle S \rangle_T$ is the mean salinity on an isothermal surface of temperature T.

Consequently by using the equation of state for seawater we can calculate potential density. Stommel's method could also have been modified and used to estimate density directly from temperature by using the mean of density on isothermals, yielding the same result.

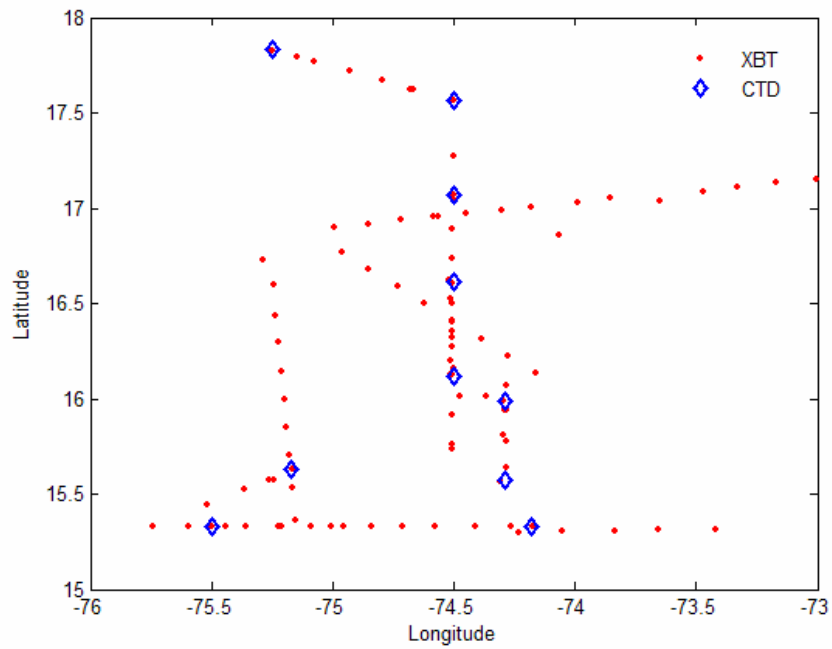


Figure 4.2 Positions of XBT deployments and CTD stations during Cavortex IV.

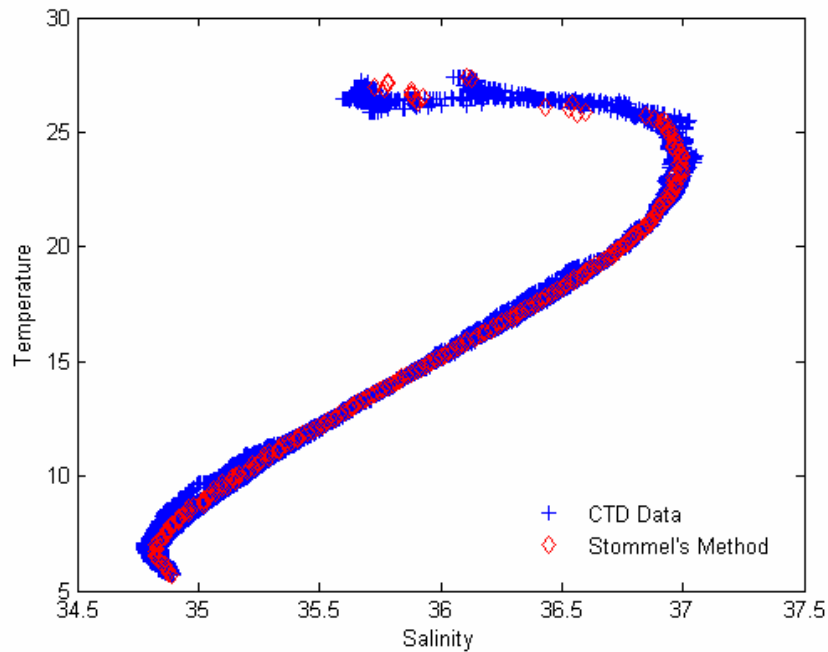


Figure 4.3 T-S relationship during Cavortex IV. Stommel's method at 0.1 C intervals compared with the actual data from the 11 CTD stations.

4.6. Estimating diapycnal diffusivity

. The vertical eddy diffusivity coefficient is very controversial, and many parameterizations exist to estimate its value. One such example is the one proposed by *Gargett (1984)* commonly used in simple OGCM's:

$$\kappa_d = \frac{3.4 \times 10^{-7}}{N} \quad (4.11)$$

where N is the Brunt-Vaisala frequency . But note that it is only dependent on the stability of the water column due to buoyancy forces created by the density field. A much better estimate would be one that takes into account both the stabilizing forces due to buoyancy and the destabilizing forces due to the vertical shear in velocity of the flow. The former can be calculated from CTD casts while the latter are calculated from LADCP data. We find such a method in the Richardson number dependent Pacanowsky-Philander vertical mixing scheme (*Pacanowski and Philander, 1981*). The vertical eddy diffusivity κ_d is parameterized as follows:

$$\kappa_d = \frac{\nu}{(1 + \alpha Ri)} + \kappa_b \quad (4.12)$$

where:

$$\nu = \frac{\nu_0}{(1 + \alpha Ri)^n} + \nu_b \quad (4.13)$$

is the eddy viscosity, ν_b and κ_b are background values, and ν_0 , α and n are empirical variable parameters. Ri is the local gradient Richardson number:

$$Ri = \frac{N^2}{S^2} = \frac{\frac{-g}{\rho_0} \left(\frac{\partial \rho}{\partial z} \right)}{\left(\frac{\partial u}{\partial z} \right)^2 + \left(\frac{\partial v}{\partial z} \right)^2} \quad (4.14)$$

where u & v are the velocity components in the east-west and north-south directions respectively. For consistency, the values used for these parameters will be the same used in the Caribbean by *Alfonso (2001)* which was cited from *Pacanowski and Philander (1981)*. This scheme, together with these values, has been extensively used in General Circulation Models, being more successful in the tropical regions. They are the following:

$$\begin{aligned}
 n &= 2 \\
 \alpha &= 5 \\
 \nu_0 &= 100(\text{cm}^2 \text{s}^{-1}) \\
 \nu_b &= 1.0(\text{cm}^2 \text{s}^{-1}) \\
 \kappa_b &= 0.1(\text{cm}^2 \text{s}^{-1})
 \end{aligned}$$

Note that the value of the eddy viscosity ν is not kept constant but varies with the value of the Richardson number. This makes for greater accuracy when estimating values for the vertical eddy diffusivity (*Pacanowski and Philander, 1981*).

Although other efficient methods of estimating vertical diffusivity exist such as KPP theory and several turbulence closure schemes (e.g. Mellor-Yamada), for the present study the *Pacanowski and Philander* method was favored due to its simplicity. It was also favored for the sake of consistency as other studies in the Caribbean have employed the same approach (*Alfonso, 2001; Morell et al., 2001; Pelaez, 2001*).

4.7 Calculation of geostrophic currents

Geostrophic theory relies on the assumptions that the pressure gradient is balanced by the Coriolis force. The equations of motion for inviscid flow under geostrophic equilibrium are:

$$-fv = -\frac{1}{\rho_0} \frac{\partial p}{\partial x} \quad (4.15)$$

$$+fu = -\frac{1}{\rho_0} \frac{\partial p}{\partial y} \quad (4.16)$$

$$0 = \frac{1}{\rho_0} \frac{\partial p}{\partial z} \quad (4.17)$$

$$\frac{\partial u}{\partial x} + \frac{\partial v}{\partial y} + \frac{\partial w}{\partial z} = 0 \quad (4.18)$$

Solving the equations 4.15 & 4.16 in terms of the horizontal velocity components yields:

$$u = -\frac{1}{\rho_0 f} \frac{\partial p}{\partial y} \quad (4.19)$$

$$v = \frac{1}{\rho_0 f} \frac{\partial p}{\partial x} \quad (4.20)$$

The above equations for u and v are used to calculate the geostrophic flow based on hydrographic data. The variables used are defined as:

ρ = density,

$f = 2\Omega \sin\phi$

$\Omega = 7.292 * 10^{-5} \text{ s}^{-1}$

ϕ = latitude

$\frac{\partial p}{\partial x}$ = pressure gradient between CTD casts

The hydrostatic equation used is:

$$\Delta D = \int_0^z \delta dp \quad (4.21)$$

Where:

$\delta = \frac{1}{\rho}$, is the specific volume anomaly

z = reference level, otherwise known as level of no motion (usually 1000 dbar)

$\partial x = \Delta x$, distance between CTD casts.

Therefore:

$$v = \frac{\Delta D}{2\Omega \sin \phi \Delta x} \quad (4.22)$$

Equation 4.22 is the one used directly to calculate the geostrophic velocity orthogonal to a straight line between the 2 stations. This straight line is taken to be the x axis, with v being the velocity in the direction of the y axis.

4.8. Satellite altimetry

Data from the AVISO website was used for the spatial analysis of the eddy field. The Near Real Time merged (Topex-Poseidon, Jason-1, GFO, Envisat and ERS-1) data set was used and contour plots were obtained from their Live Data Server interface at <http://las.aviso.oceanobs.com/las/servlets/dataset>. The final product, Mean Sea Level Anomaly, which contains merged data from all 5 satellites, was used extensively in the visual analysis of the eddies in this study.

4.9 Nu-Shuttle undulating vehicle

High resolution, almost continuous profiles of the near surface layer (0-90 meters) were obtained using a Chelsea Instruments undulating underwater vehicle (Nu-Shuttle). This data set provides a unique method of sampling that can resolve small scale features

and shed light on interactions at multiple scales. This vehicle is towed behind the ship at full speed (~10 knots) while it undulates from 30-90 meters in a sinusoidal fashion. It was equipped with a Minipack CTD, an optode, a phycoeritrin sensor and a fast repetition rate fluorometry (FRRF) sensor.

5. Results and Discussion

The results for each feature are presented separately and are discussed within the context of their three-dimensional structure. The issues of their formation and movement, their thermal, salinity, density and velocity structure are addressed using in situ and satellite data. Then the similarities and differences between the features are compared in terms of the results.

5.1 The Cyclone

A large, energetic cyclone was visited from August 8-15, 2003 aboard the R/V Chapman. Several CTD stations were occupied meridionally across the eddy, and XBT's were launched during transit between stations. Both ocean color imagery (*Figure 5.1.1*) and satellite altimetry (*Figure 5.5.2*) indicated its existence, which was verified by in-situ observations (see *Corredor et al., 2004*).

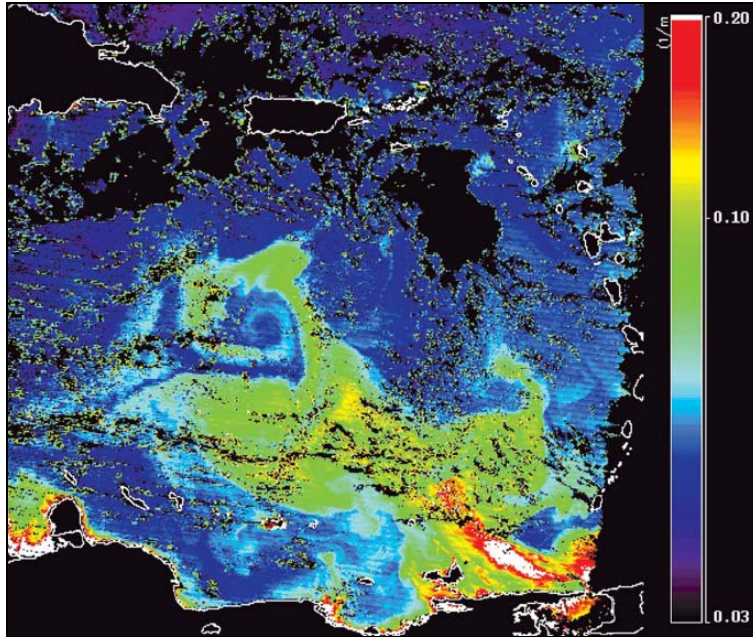


Figure 5.1.1 K490 MODIS image of the cyclonic eddy. Notice the advection of the Orinoco River Plume by the structure.

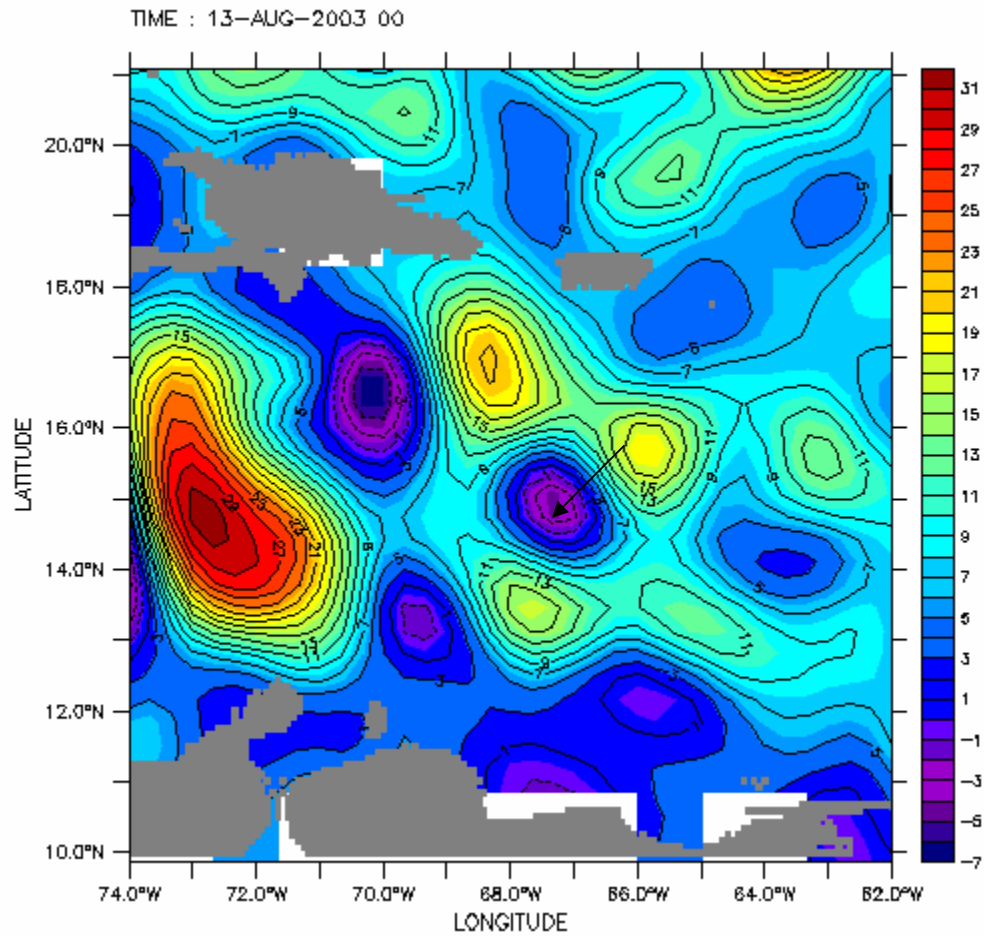


Figure 5.1.2 AVISO altimetry for August 13, 2003. The arrow indicates the location of the center of the eddy.

5.1.1 Formation, Development and Motion

SSHA plots give insight into the formation mechanism of this cyclonic eddy. It seems a patch of cyclonic vorticity that advected into the Caribbean was intensified by the impingement of an anticyclone into the Lesser Antilles. This patch of cyclonic vorticity was traveling to the west of an anticyclone. As they were advected westward, the anticyclone did not enter the Caribbean, but traveled meridionally along the Lesser Antilles. This is consistent with numerical modeling results (*Simmons and Nof, 2001*) that show small, intense NBC rings are less likely to enter the Caribbean than larger, weaker ones. The cyclonic vorticity did enter, and strengthened possibly feeding off the cyclonic shear created by the anticyclone trying to enter the Caribbean (*Figure 5.1.3*). This is consistent with the numerical modeling results of *Carton and Chao (1999)*, that cyclonic circulation is produced to the west of an NBC ring after interacting with the Lesser Antilles. This advected vorticity may have acted as a finite amplitude perturbation that has been shown to create mixed barotropic and baroclinic instabilities that can amplify or generate mesoscale features in the Caribbean (*Murphy et al., 1999*). The generation of this eddy seems to agree with the findings of *Richardson (2005)* that Eastern Caribbean cyclones usually lie or begin near topographic features of the basin.

Satellite ocean color imagery revealed the advection of the Orinoco river plume by the eddy (*Figure 5.1.1*). The water was entrained inside the eddy in a spiral pattern. Because cyclonic eddies present divergent surface flow, in theory an ideal eddy should have traversed the ORP as a clear disk. But because it presented this entrainment, the only way to explain this phenomenon would be that the ORP water was trapped inside the eddy during formation and/or strengthening. Because the point of apparent formation

is within the meridional extent of the ORP, as the cyclone formed it likely entrained the ORP water and carried it along its voyage into the middle of the Caribbean. Slowly but surely the ORP water was turbulently diffused across the Caribbean.

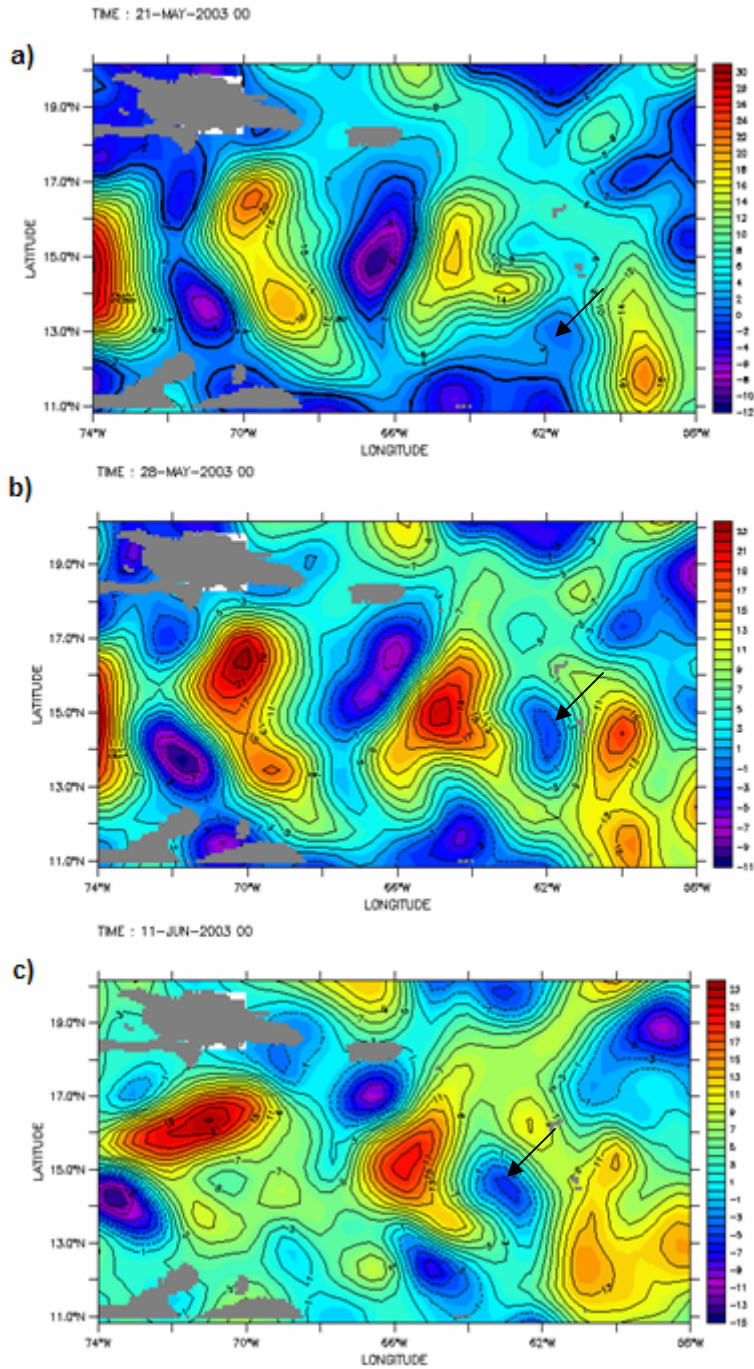


Figure 5.1.3 AVISO altimetry shows the apparent formation of the cyclone. (a) An anticyclone collides with the Lesser Antilles and induces a cyclonic circulation on its western side, the cyclonically sheared side. (b) A small cyclone apparently forms as a result of the strengthening of advected vorticity and interacts with adjacent eddies. (c) The cyclone is advected westwards across the Caribbean. By August 13, 2003 the eddy had increased both in size and in amplitude (Figure 5.2.2).

5.1.2 Hydrography

A hydrographic section from CTD casts (*Figure 5.1.4*), as well as XBT temperature data (*Figure 5.1.5*) revealed a strongly baroclinic structure, with shoaling of isopycnals and isothermals occurring in the top 700 meters of the water column. Deeper than this level, isopycnals showed no sign of shoaling; indicating that the vertical effects of this feature on the density structure of the water column was limited. Vertical displacement of isopycnals showed amplitudes as large as 50 meters in the center of the eddy. This uplift brings cold, nutrient rich water into the euphotic zone that can significantly enhance biological production (*McGillicuddy et al., 1998*), a process that has been called “eddy pumping”.

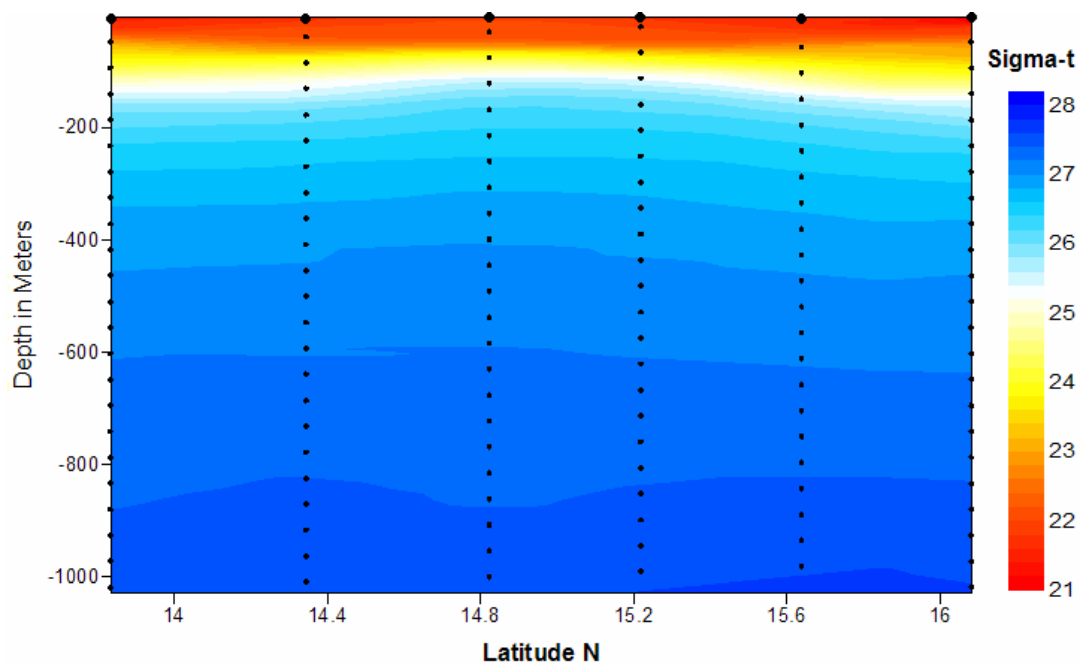


Figure 5.1.4 Density (σ_t) structure of the eddy shows shoaling of isopycnals in the top 700 meters of the water column.

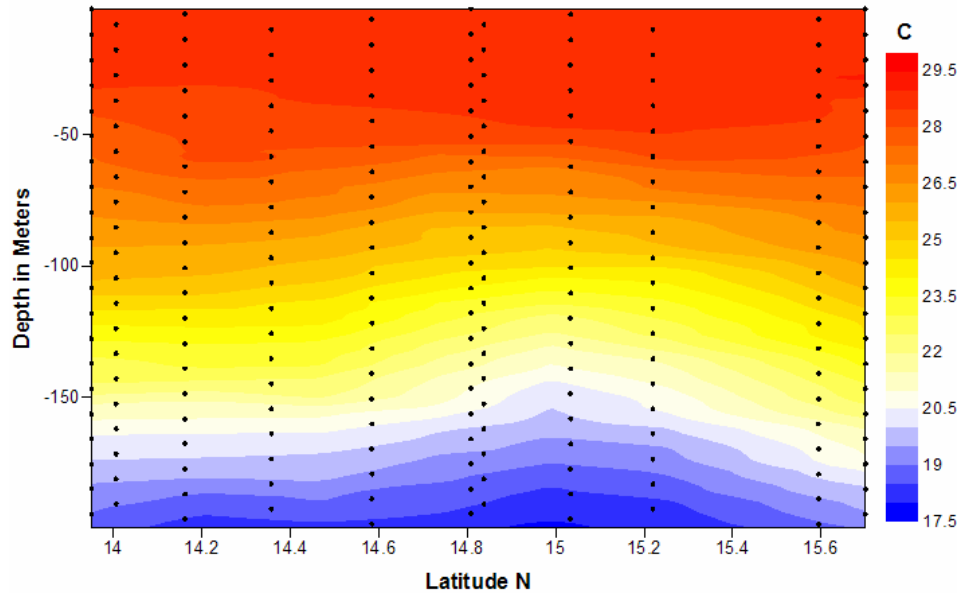


Figure 5.1.5 XBT temperature section of the top 200 meters shows shoaling of isotherms indicating upwelling in the center of the eddy.

Indeed, chlorophyll fluorescence was significantly enhanced in the center of the eddy, a region that coincides with the shoaling of nutrient rich isopycnals (*Figure 5.1.6*).

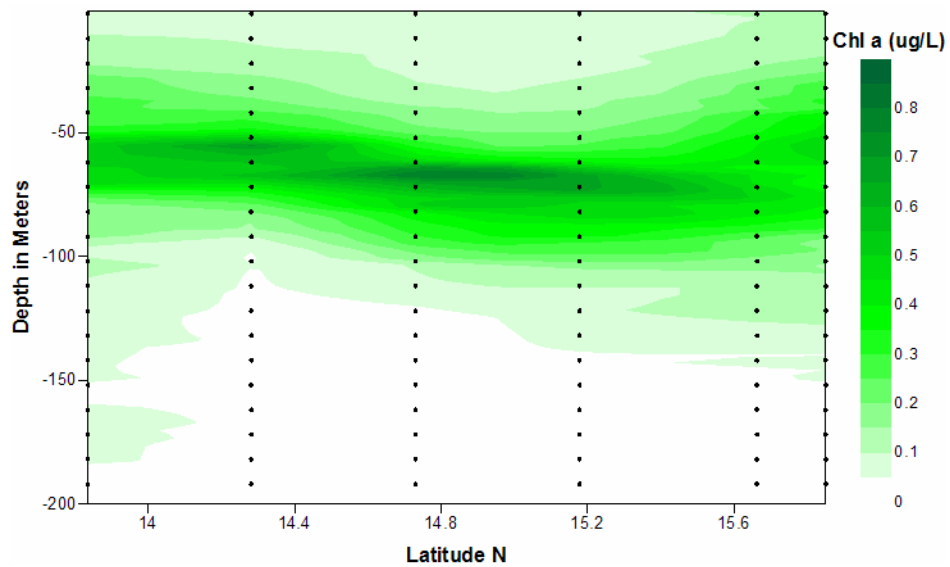


Figure 5.1.6 Chlorophyll a concentration (ug/L) shows an increase of phytoplankton activity in the center of the eddy, around 15 N.

The salinity structure was somewhat more complex, due to the presence of saltier, oceanic waters in the eddy core, which displaced the buoyant, low salinity plume waters. A ring of low salinity water can be seen surrounding the more saline, oceanic core of the eddy (*Figure 5.1.7*). The Subtropical Underwater (SUW) mass can be identified by the salinity maximum around 150 meters. The SUW mass itself is uplifted about 40 meters by the upwelling in the center of the eddy.

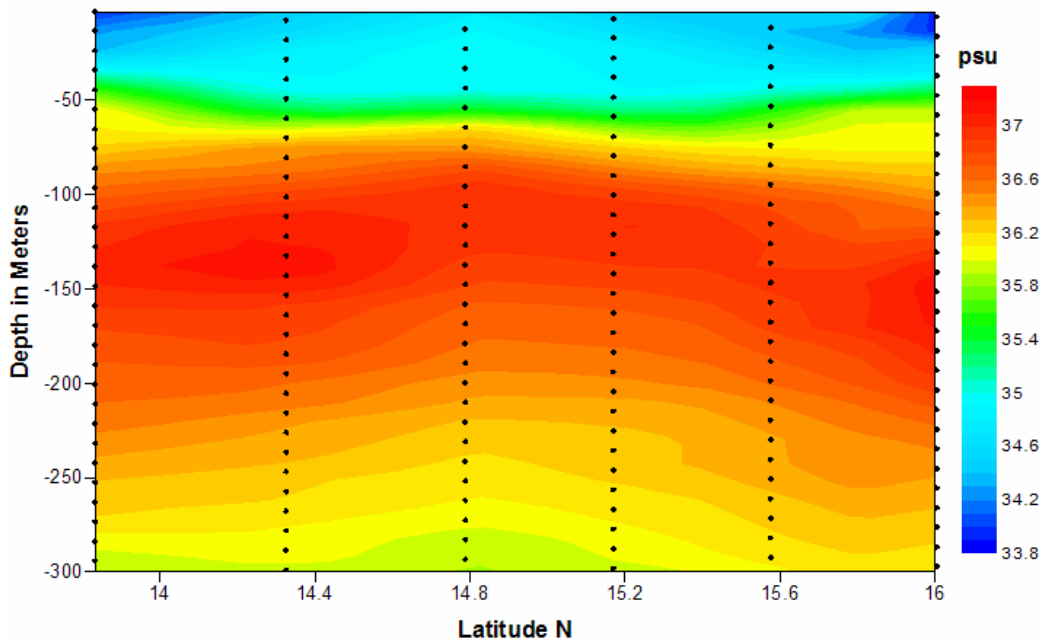


Figure 5.1.7 Meridional section of practical salinity shows a ring of low salinity water around the saltier, oceanic core of the eddy. This is the Orinoco River Plume water being advected by the cyclone as seen in Figure 5.1.1.

Thermohaline staircases were evident within the eddy, but were much better defined in the edges of the eddy. Both the northern and southern edges presented this phenomenon, which has been implicated in enhanced diapycnal mixing (*Schmitt et al., 2005*).

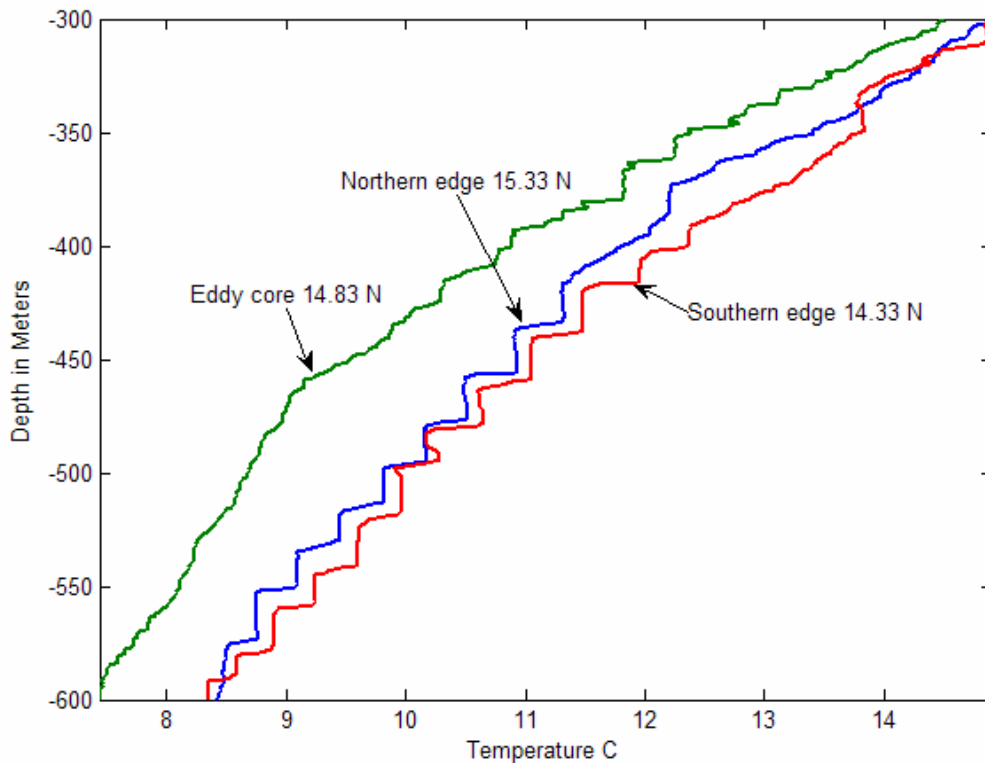


Figure 5.1.8 Temperature staircasing at different stations within the eddy. Well defined staircases are missing in the eddy core station.

5.1.3 Velocity Structure

Geostrophic currents calculated using the CTD profiles revealed a counterclockwise rotation typical of northern hemisphere cyclones (*Figure 5.1.8*). Swirl velocities as large as 40 cm/s are seen both to the north and south of the eddy. Because the cruise track was north to south, this calculated velocity can be considered the zonal component of the geostrophic velocity of the cyclone.

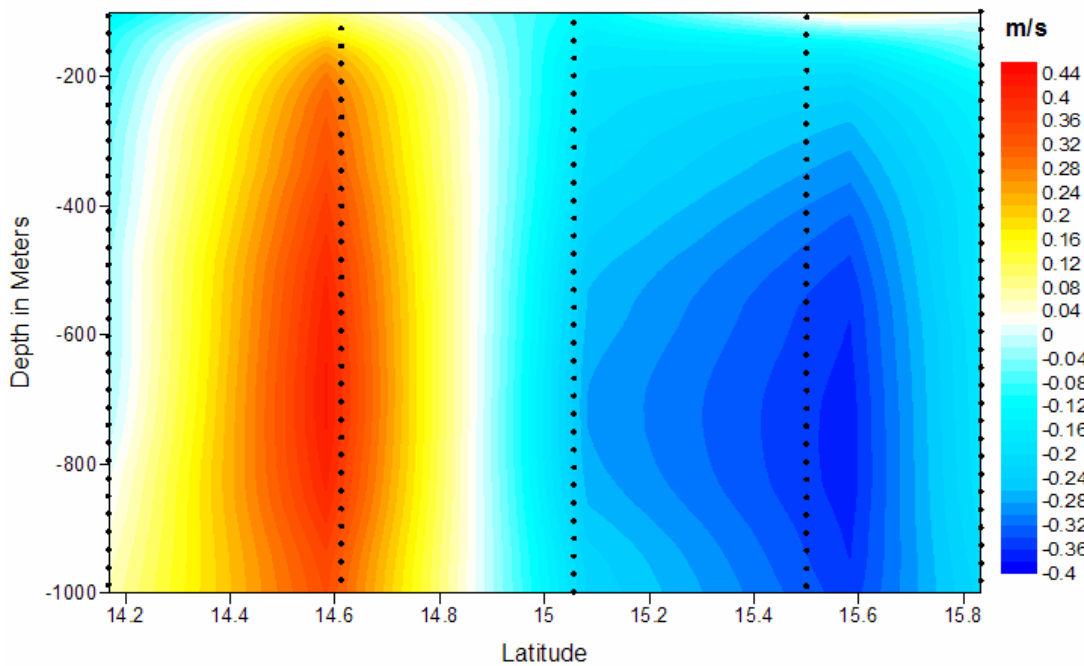


Figure 5.1.9 Geostrophic velocity along a meridional section across the eddy shows cyclonic rotation with maximum velocities of 40 cm/s. Because the track was N-S, this velocity can be considered as the u-component of the geostrophic flow of the eddy.

5.2 The anticyclone

An energetic anticyclone was visited during Cavortex IV from March 12-25, 2005 aboard the R/V Pelican. It was an asymmetric, meridionally elongated eddy that was undergoing a rapid deformation phase, propagating southwestward along the Jamaica ridge while being advected by the Caribbean Current at about 14 N. During a span of about three weeks, the eddy evolved from a meridionally elongated structure to a more circular one, apparently merging with a companion anticyclone to its south (*Figure 5.2.1*).

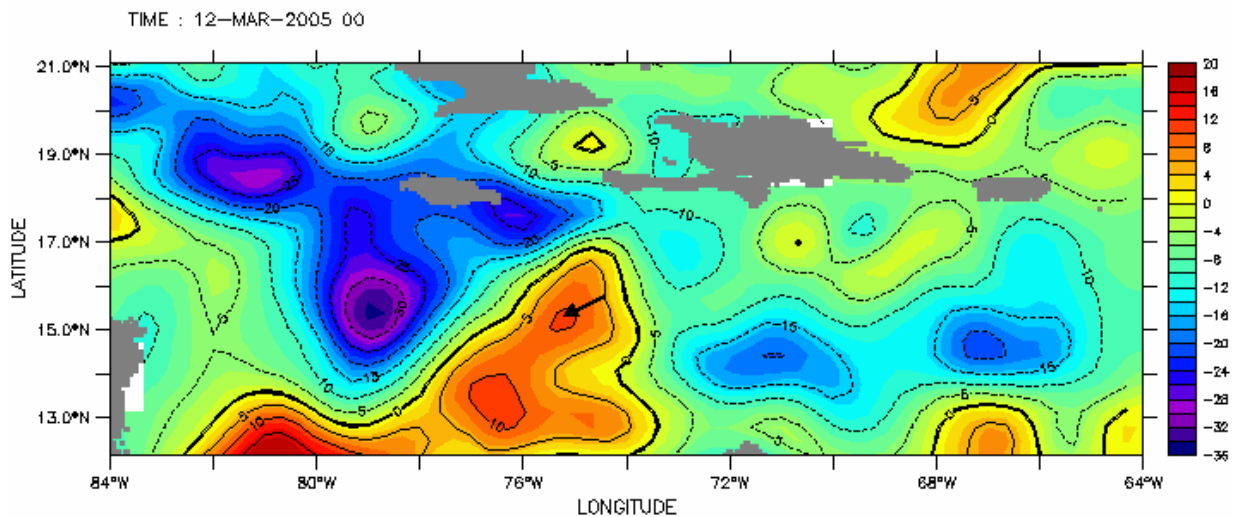


Figure 5.2.1 AVISO merged altimetry for March 12, 2005 showing the area of the study. The arrow indicates the anticyclone that was surveyed.

At the time of the survey, its meridional extent was about 300 km in diameter and its zonal extent was about 250 km before the merging event.

5.2.1 Formation, development and motion

Around the middle of September, 2004, SSHA plots showed a small anticyclone-like structure squeezing into the Caribbean Sea through or near the Anegada Passage (Figure 5.2.2).

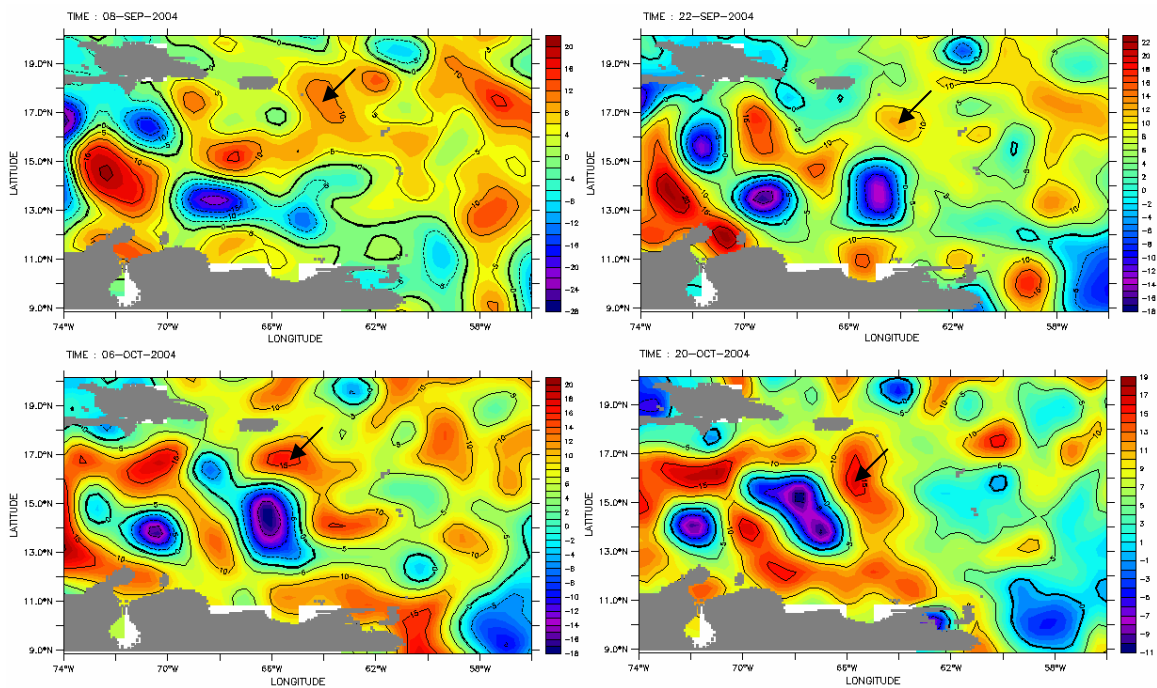


Figure 5.2.2 AVISO altimetry shows an area of anticyclonic vorticity apparently squeezing into the Caribbean Sea through the Anegada Passage. Arrows show its location at each image taken at two week intervals. This eddy would strengthen considerably by the time it was surveyed in March 2005 southeast of Jamaica.

This structure then proceeded to propagate southwestward, and by the end of October it was located about 200 miles south of Puerto Rico. Coincidentally, the Caribbean Time Series station, which lies more than 20 nautical miles off southwestern Puerto Rico, was occupied during this time. SSHA plots confirmed CaTS was at least partially under the influence of the eddy (Figure 5.2.3). The effects of the anticyclone seem to have been recorded in the LADCP velocity profile, which showed a southeast flow in the upper 150 meters, which coincides with the direction of the current

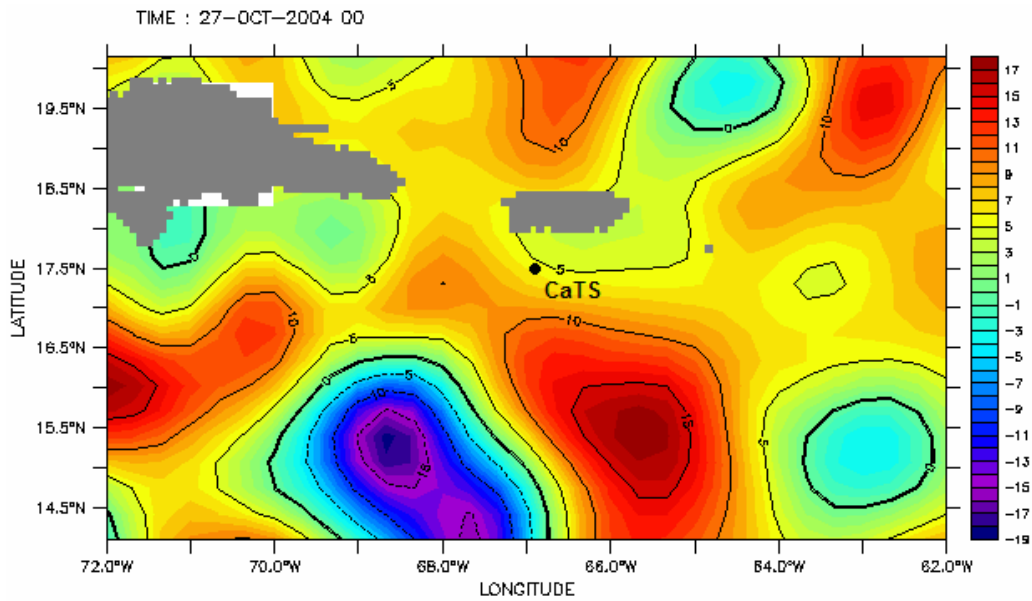


Figure 5.2.3 AVISO merged altimetry for October 27, 2004 shows the proximity of the anticyclone to Puerto Rico that was eventually surveyed on March 2005 southeast of Jamaica.

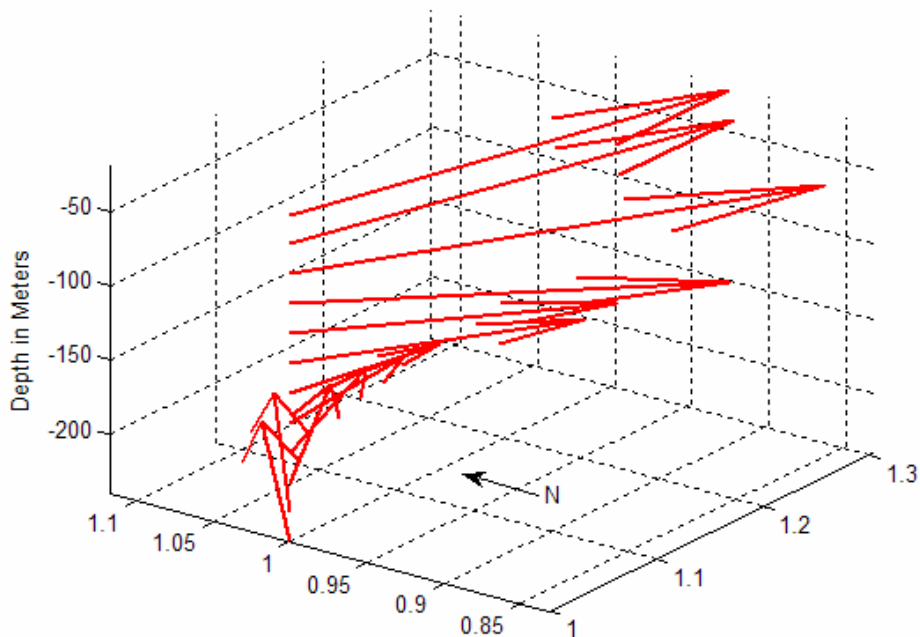


Figure 5.2.4 LADCP velocity profile on October 22, 2004 at the Caribbean Time Series shows a strong southeast flow in the upper 150 meters. The largest arrow represents a velocity of 37 cm/s. This direction coincides with the direction of the SSHA isolines in Figure 10 suggesting the effects of the eddy were measured at CaTS.

in the NE portion of an anticyclone (*Figure 5.2.4*). So it seems the eddy was indirectly sampled five months earlier and more than 1000 kilometers from where it was studied in detail near Jamaica.

The eddy continued advecting to the west at about 10 cm/s, passing 100 miles to the south of the Mona Passage. Afterwards the SSHA signal weakened significantly for a time period of at least a month. It is not clear if this was a result of satellite sampling error or a weakening of the structure itself. If it was indeed a weakening, some process may have extracted energy from the eddy. The Mona Passage is the shallowest major passage in the Antilles, with a sill depth of 400 meters and provides an inflow of about 3 Sv into the Caribbean (*Johns et al., 2002*). Whether this flow may have had an effect on the apparent weakening remains a mystery, yet it is an interesting possibility to consider. The eddy continued westward and advected over the Beata Ridge, and shortly after this it's SSHA signal strengthened. This area has been identified as a hot spot of eddy formation and/or intensification due to anticyclonic wind stress curl (*Andrade and Barton, 2000, Oey et al., 2003*). After this the eddy advected southwestward and increased its propagation speed more than 12 cm/s. It continued this course until it apparently merged with another anticyclone to its south and formed a very large anticyclone by the end of March.

5.2.2 Hydrography

The density structure obtained from the CTD casts shows deepening of isopycnals in the center of the eddy (*Figure 5.2.5*). Displacements as large as 40 meters occur on some isopycnals. It is particularly interesting that the amplitude of the displacement of isopycnals is significant in the upper 150 meters. Then isopycnals appear almost flat, only to start shoaling significantly again below 500 meters.

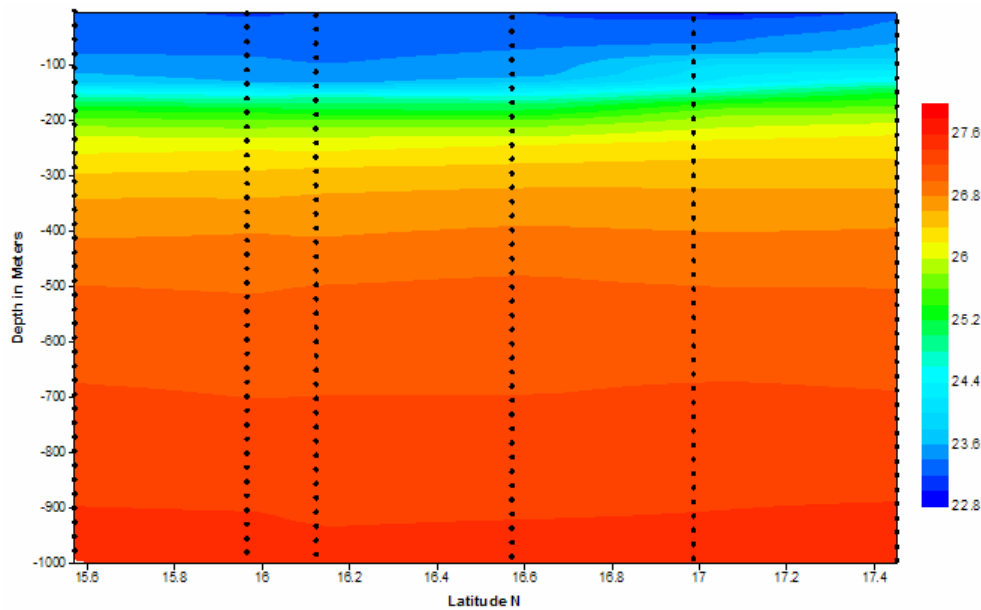


Figure 5.2.5 Meridional transect of sigma-t shows the effects of the eddy on the density structure as deep as 1000 meters.

XBT temperature data showed similar deepening of isotherms. The temperature distribution at 200 meters of depth shows warmer water in the middle and towards the southwest of the inferred center of the eddy (*Figure 5.2.6*). This pattern is consistent with what was inferred from SSHA plots, that the anticyclone was merging with another to its south. This is especially evident from the bottom left corner of *Figure 5.2.6*, which shows unusually warm water in a pattern similar to the SSHA in *Figure 5.2.1*. The three-dimensional thermal structure was constructed using the more than 100 XBT profiles and

interpolated using a routine written in Matlab, that had the *griddata3* command as its principal component. This command fits a hypersurface of the type $w = f(x, y, z)$ to tetradimensional (x, y, z, T) data. The topology of the 22 degree isotherm, obtained using a more complex routine involving the *patch*, *isosurface* and *isonormal* commands, suggests that the eddy was merging (Figure 5.2.7).

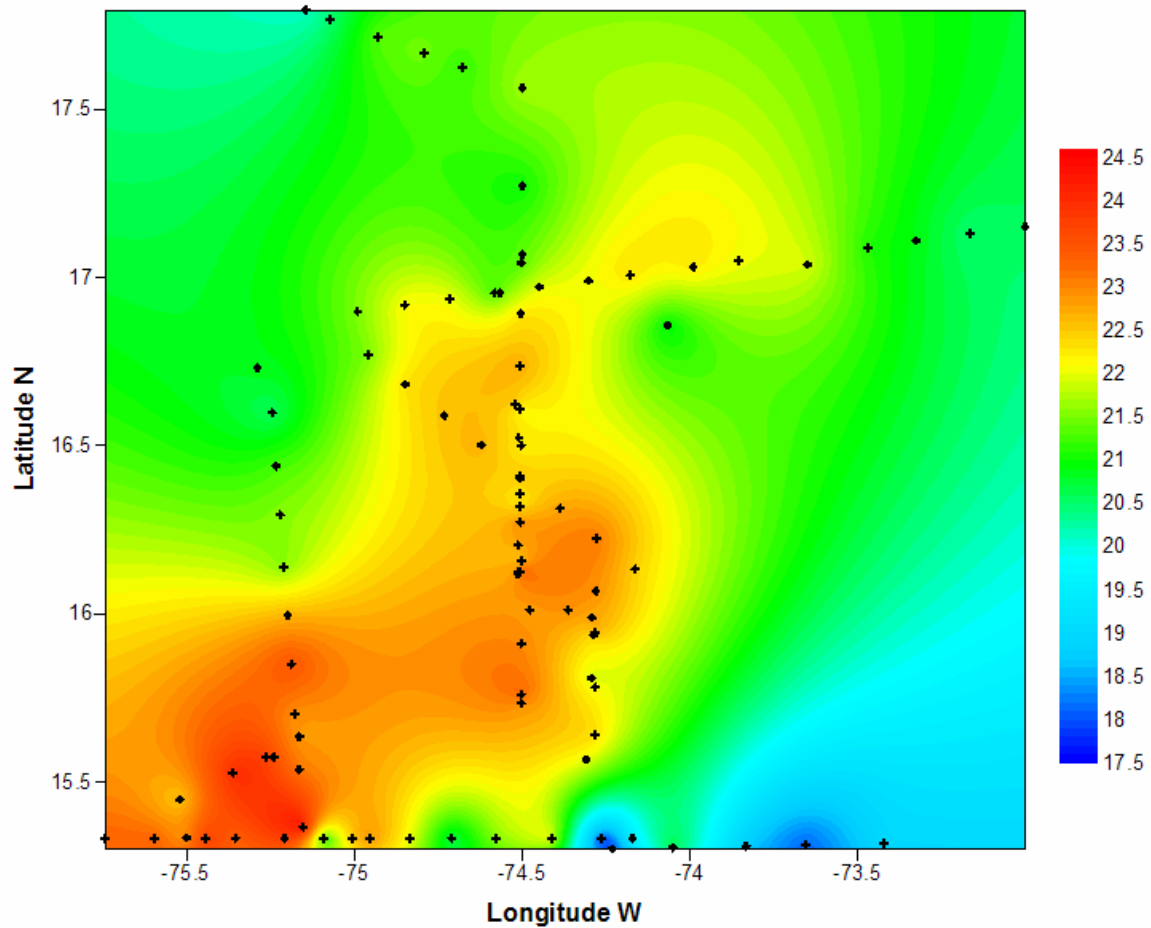


Figure 5.2.6 Temperature (in degrees Celsius) distribution at 200 meters from XBT data. Black dots denote XBT drop locations.

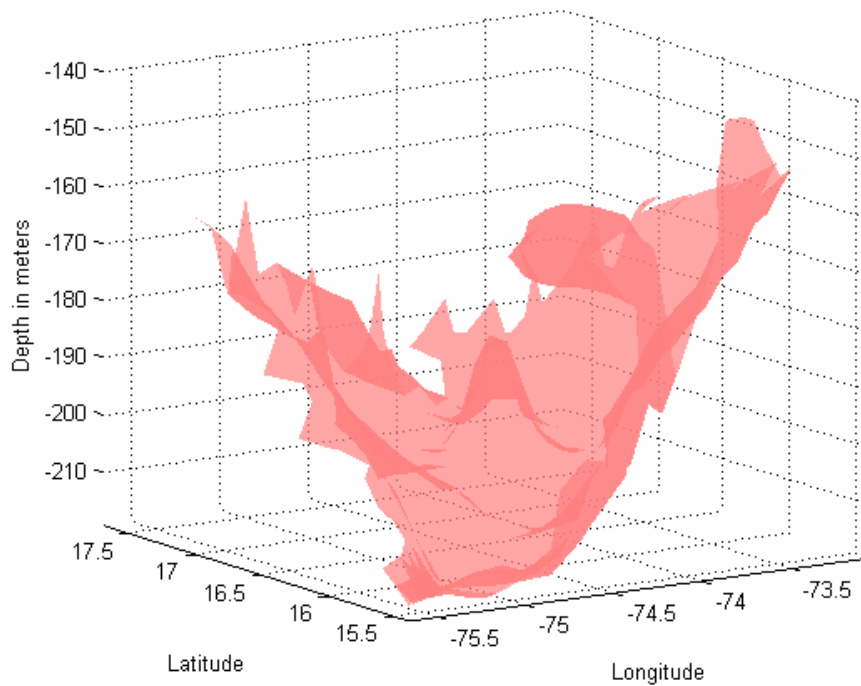


Figure 5.2.7 *Topology of the 22 °C isotherm shows deepening towards the southwest. This presents more evidence that suggests the eddy was indeed merging with another anticyclone during the time period of the survey.*

The three-dimensional density structure of the eddy was obtained using the estimated salinity from the T-S relationship found during the cruise and from XBT temperature data (see section 4.5). It was constructed using the same process as the three-dimensional thermal structure. It shows deepening of isopycnals with amplitudes as large as 50 meters near its center. The greatest isopycnal displacements are not found at the inferred center of the eddy as would have been expected. They were found near 15.5 N, 75.5 W, presenting further evidence that the eddy was merging with another anticyclone (Figure 5.2.8).

Upwelling at the southeastern edge caused by the strong shear can be seen, with chimney like structures appearing in XBT and Nu-Shuttle data. Here isopycnals are displaced as much as 100 meters relative to surrounding waters.

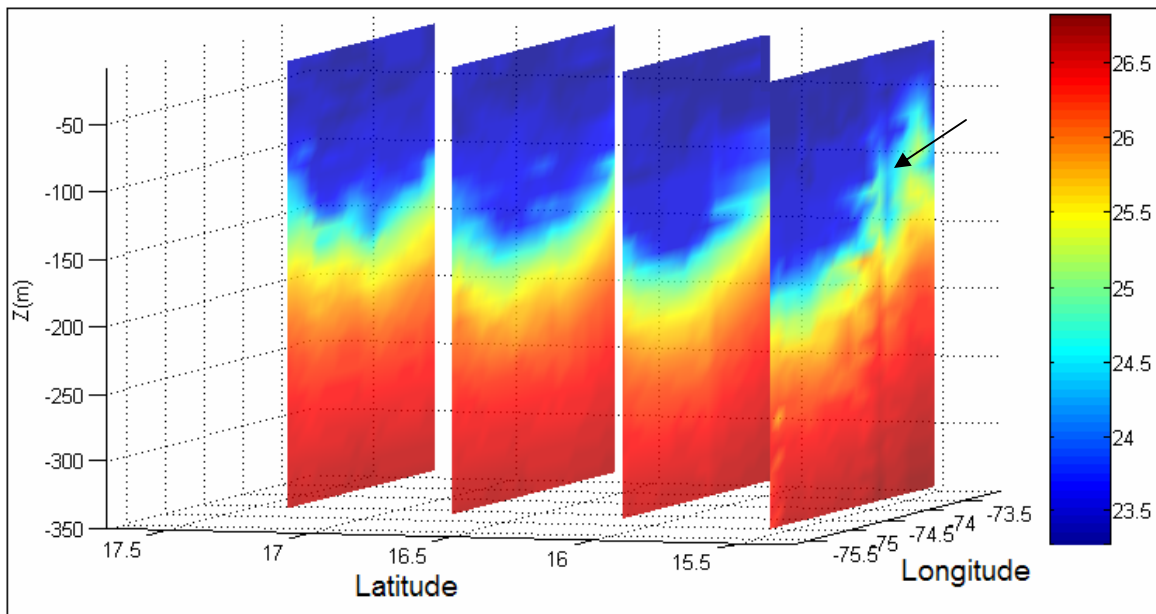


Figure 5.2.8 Three-dimensional plot of potential density calculated from the estimated salinity and XBT temperature shows deepening of isopycnals in the meridional and zonal sections. The arrow indicates the cyclonically sheared side of the eddy where density inversions are present.

This has a large impact on the chlorophyll distribution as shown by Nu-Shuttle data. The zonal section of chlorophyll fluorescence along the cyclonically sheared southeast corner shows a significant increase in phytoplankton activity, where the upwelling was present (*Figure 5.2.9*). The meridional section of the same variable shows an increase in fluorescence on the northern and southern edges of the eddy (*Figure 5.2.1*).

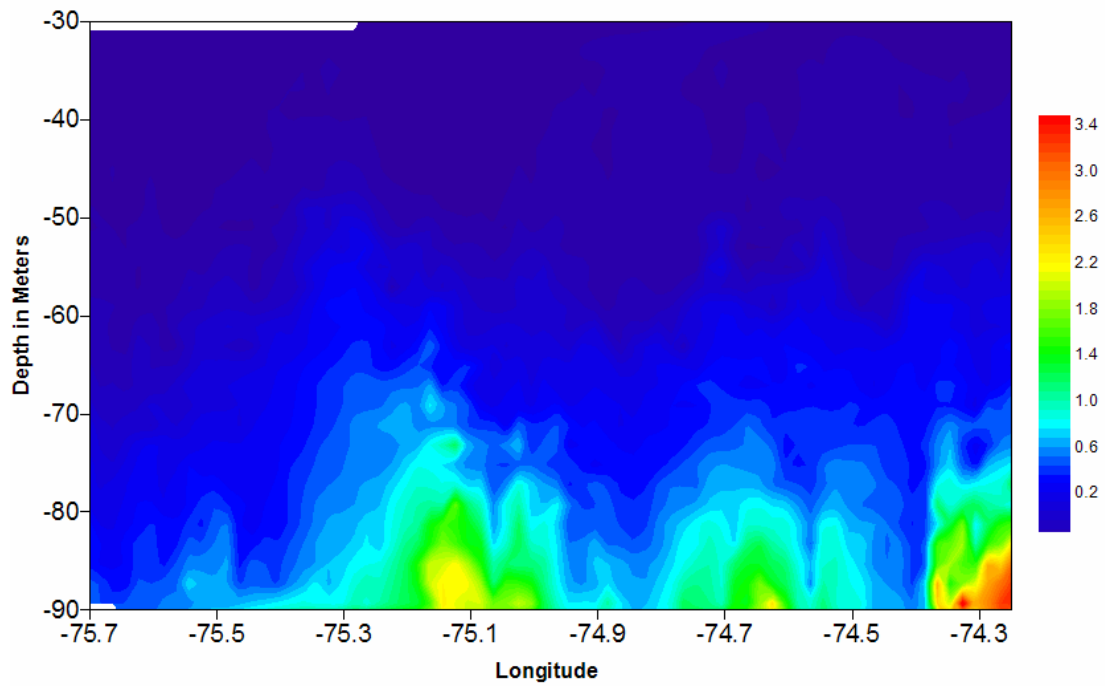


Figure 5.2.9 Zonal section of Nu-Shuttle chlorophyll a fluorescence at the southeastern, cyclonically sheared side of the eddy.

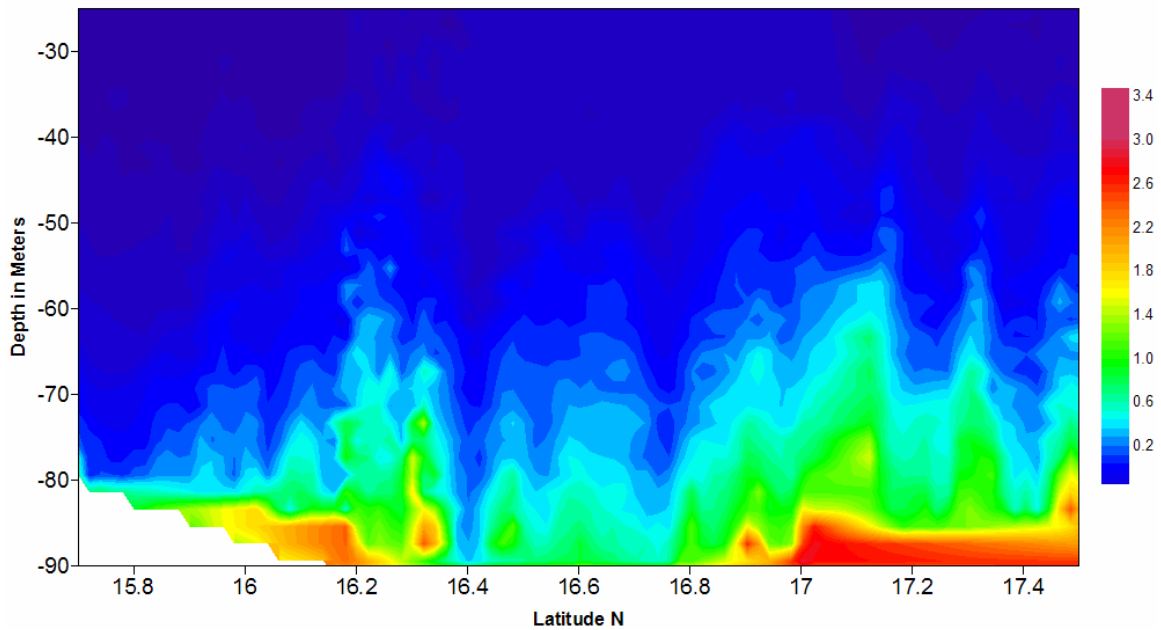


Figure 5.2.10 Meridional section at ~ 74.5 W of Nu-Shuttle chlorophyll a fluorescence along the center of the eddy shows an increase in fluorescence in the edges of the eddy at about 16N and 17.1 N.

Temperature staircases were particularly evident in the southeastern edge of the eddy (*Figure 5.2.11*). This is the zone of greatest shear and where upwelling and density inversions were evident. The eddy core did not present well formed staircases and neither did the northern edge. Three of the southern edge stations did show some well defined staircasing.

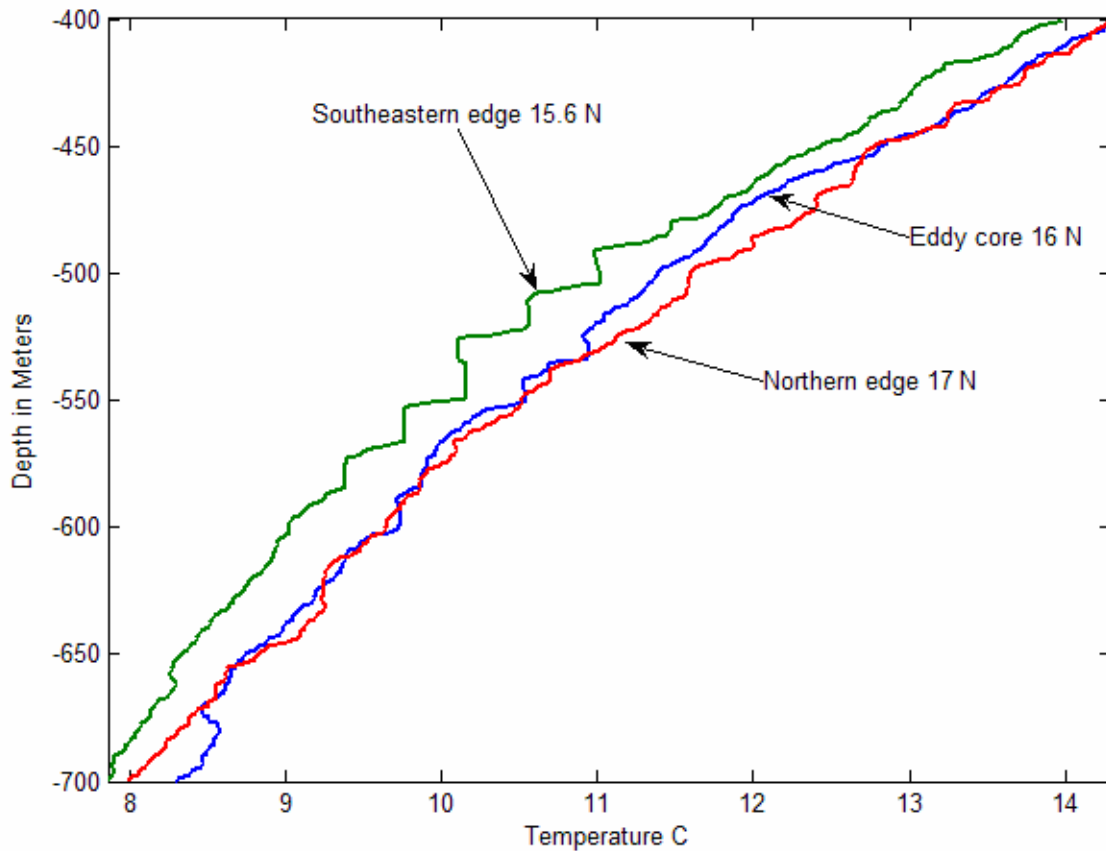


Figure 5.2.11 Temperature staircasing in different zones within the eddy. The staircases are much better defined in the southeastern edge.

5.2.3 Velocity Structure

The calculated geostrophic velocity shows anticyclonic circulation with a swirl maximum of 30 cm/s in the north and 40 cm/s in the south. The weak geostrophic flow in the top 600 meters of the southern side may be due to a decrease in the slope of isopycnals, which would cause a decrease in the pressure gradient and hence a weaker flow. This may be due to the possibility that the eddy was merging which would cause a smaller isopycnal slope as compared to a symmetric eddy.

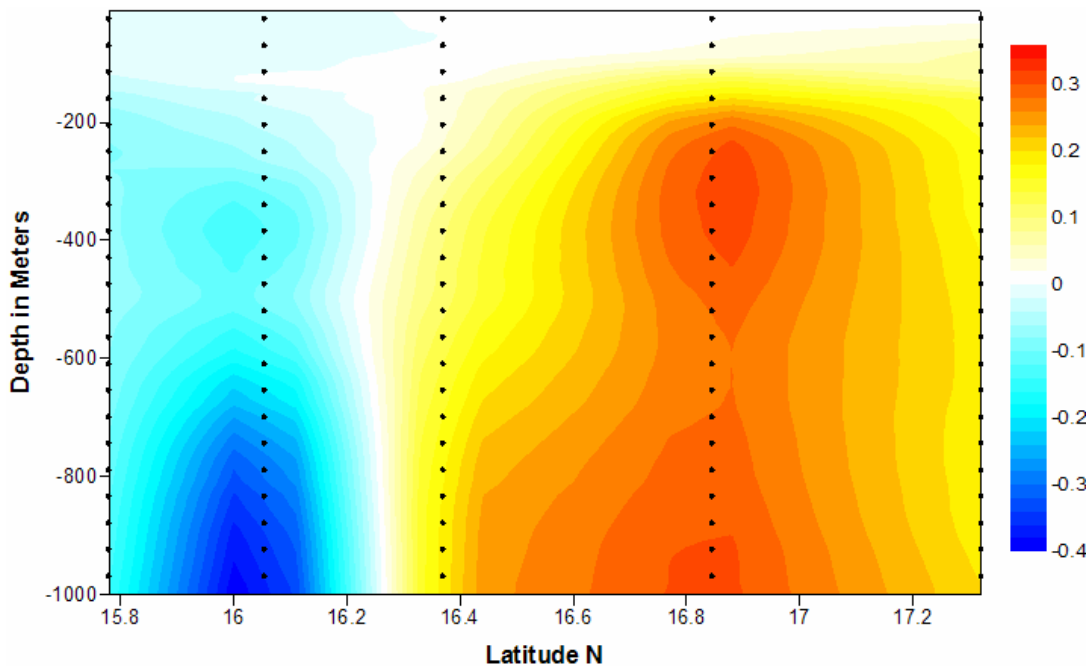


Figure 5.2.12 Meridional transect of geostrophic velocity along ~ 74.5 W shows anticyclonic circulation. Positive values indicate a current towards the east.

Direct velocity measurements revealed a surface intensified velocity structure. Radial speeds were as strong as 80 cm/s at the cyclonically sheared southern edge, but these strong velocities were confined to the upper 200 meters (*Figures 5.2.12 & 5.2.13*).

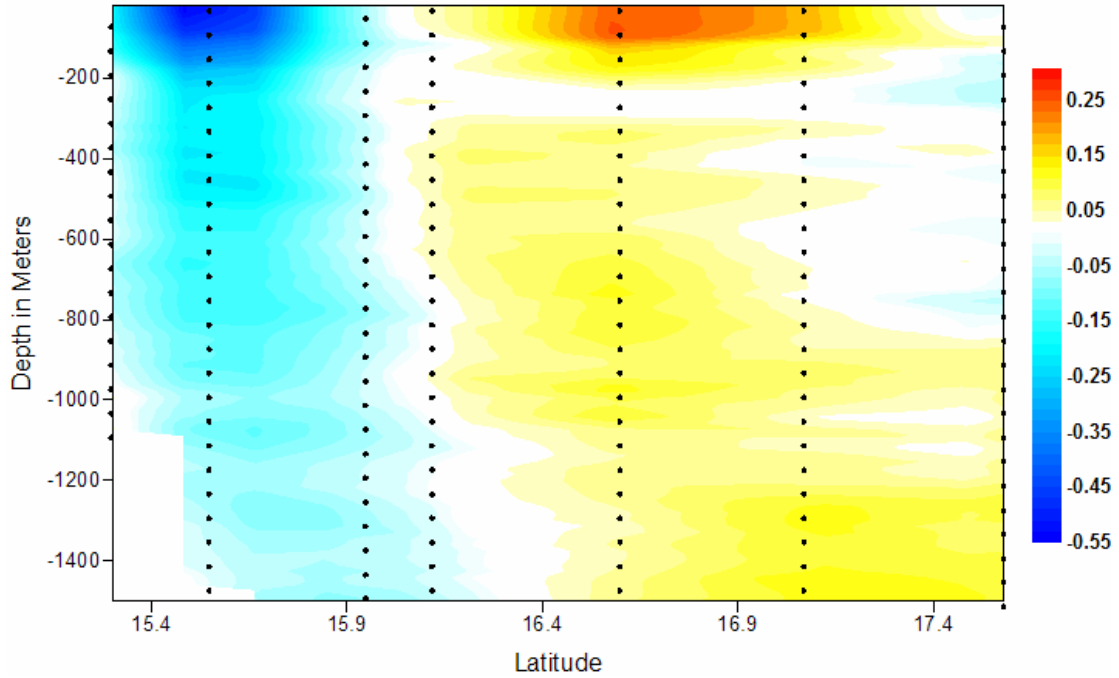


Figure 5.2.13 Meridional transect along 74.3 W of the zonal velocity component in ms^{-1} . The strongest velocities are confined to the upper 200 meters, yet its anticyclonic structure remains coherent well beyond 1400 meters.

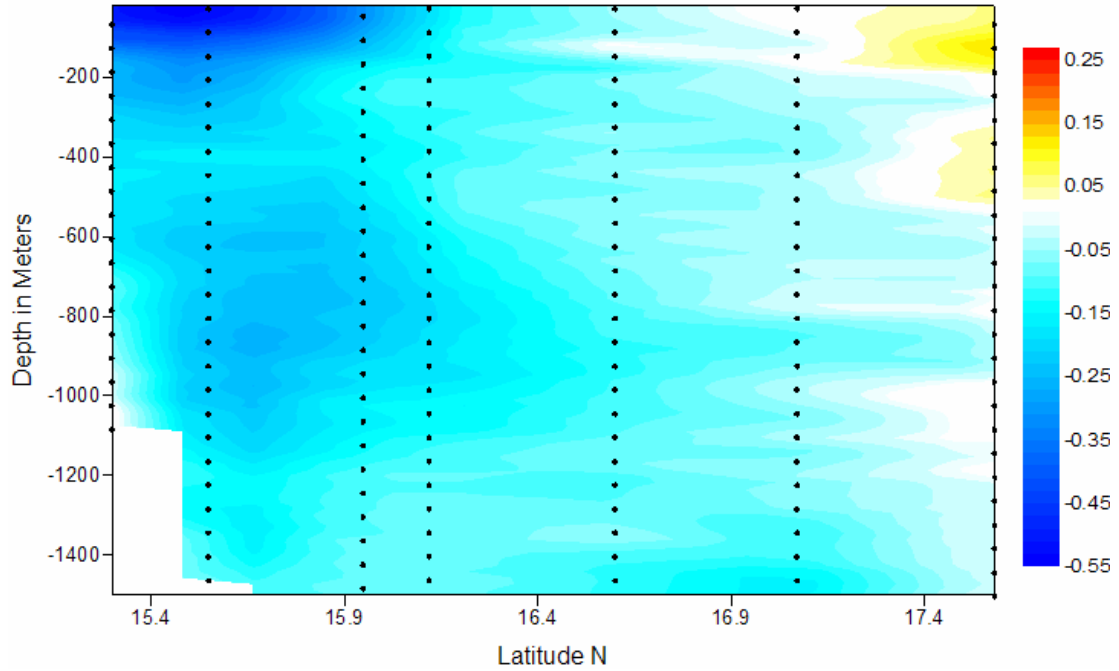


Figure 5.2.14 Meridional transect along ~74.3 W of the meridional velocity component in ms^{-1} .

This suggests that these large velocities may have been due to a combination of the rotation of the eddy, its westward advection and wind driven currents. Averaged velocity over the mixed layer, 100-500 m, 500-1000 m and 1000-1500 layers show different circulation patterns (*Figure 5.2.14*). The mixed layer flow presents stronger velocities and more circular flow. The deepest layer looks as if it were rotating with a larger radius, as the flow is less circular and more meridionally elliptic. The reason for this is not clear, although a possible explanation may be that the merging of the eddies is occurring at these greater depths. But this is entirely speculative.

The vertical shear of the current was greatest in the thermocline as is usually found in the tropical ocean (*Figure 5.2.15*). The southern edge of the eddy presents the greatest shear. This is the same area that presented upwelling and density inversions in *Figure 5.2.8*. This area is also found to have the largest diapycnal diffusivity (*Figure 5.2.16*), with values as large as $10^{-2} \text{ m}^2\text{s}^{-2}$. The combination of reduced stratification and high current shear in this zone are responsible for the enhanced diffusivity. The presence of well defined thermohaline staircases in the southeastern edge may contribute to greater diapycnal mixing, as has been found in tracer injection experiments in the Tropical Atlantic (*Schmitt et al., 2005*).

The three dimensional velocity structure of the eddy, overlaid with AVISO SSHA data is shown on *Figure 5.2.17*.

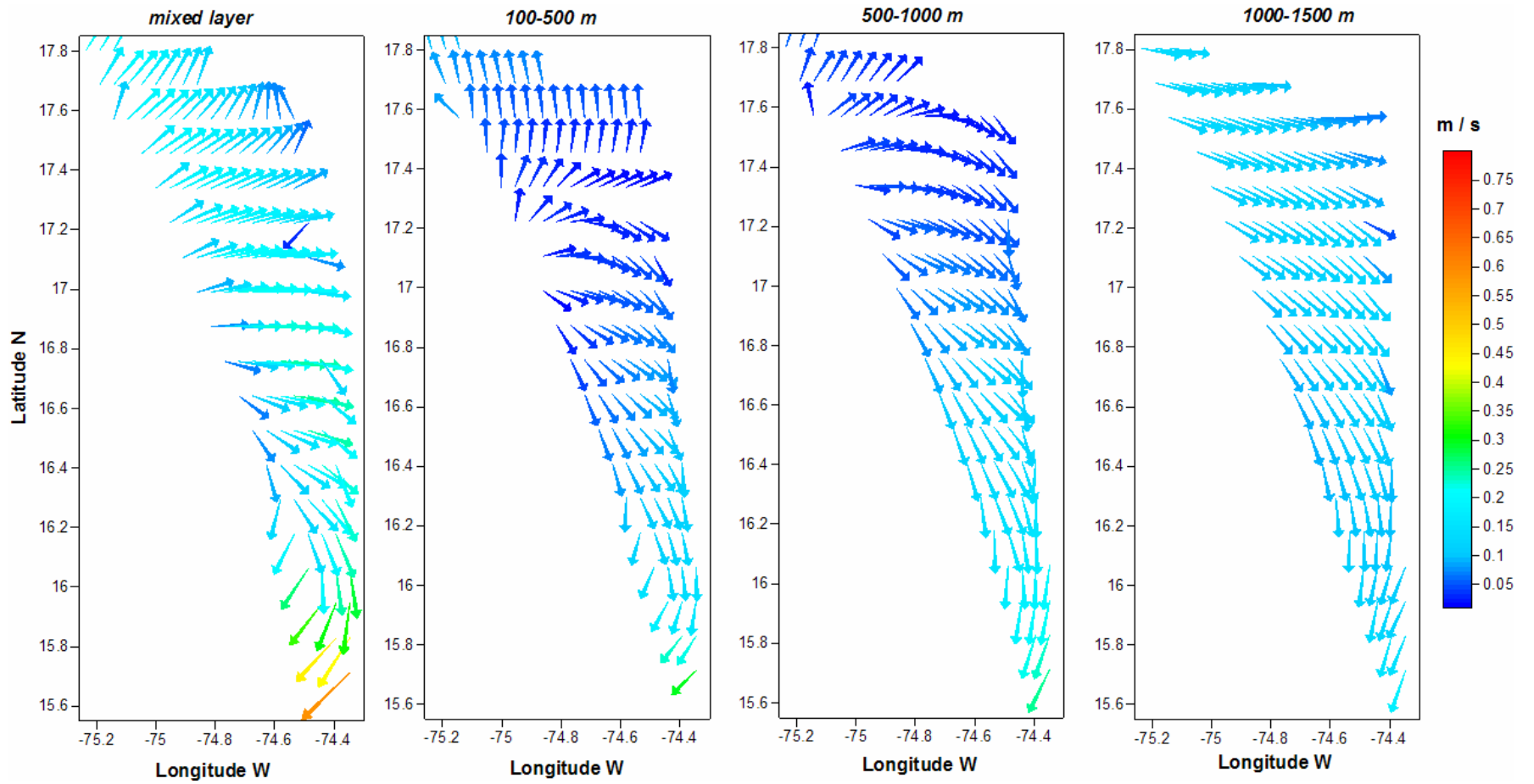


Figure 5.2.15 Average velocity distribution at different layers.

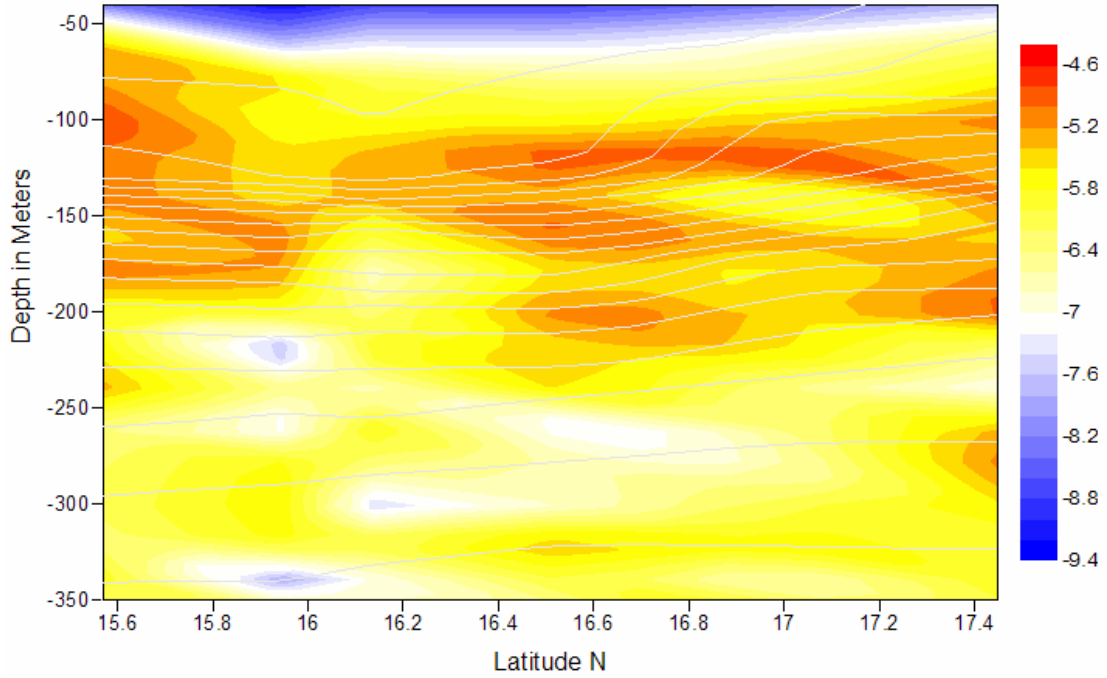


Figure 5.2.16 Contour plot of the base 10 logarithm of current shear squared (in s^{-2}). Overlaid on the figure are sigma-t density contours.

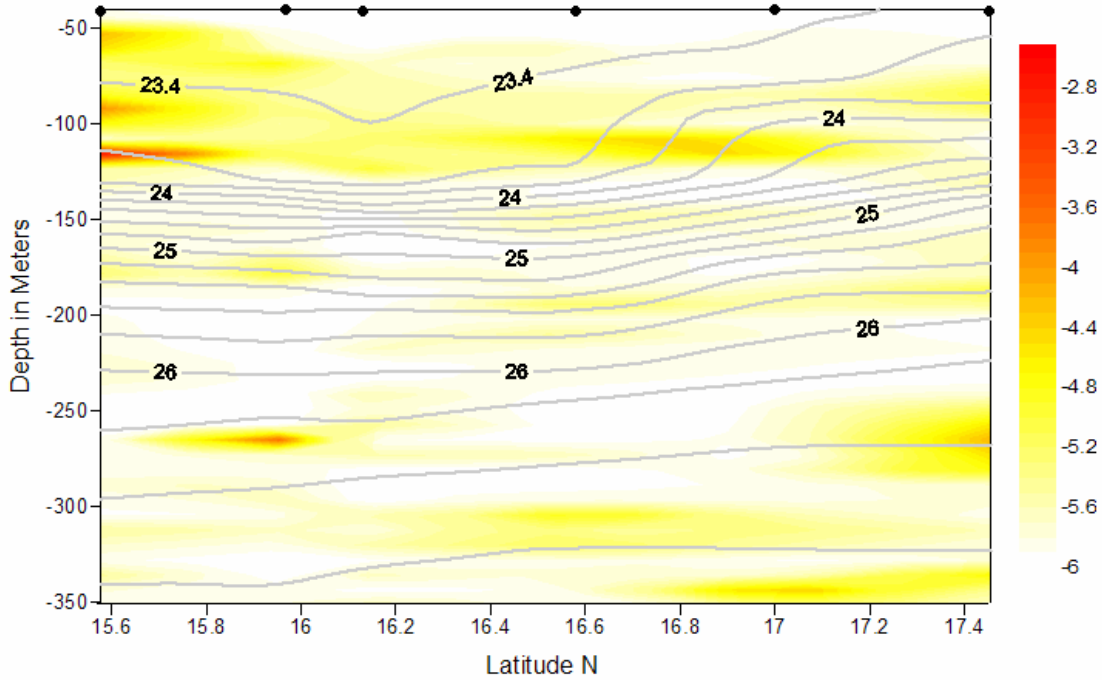


Figure 5.2.17 Meridional transect of estimated \log_{10} diapycnal diffusivity (in $m^2 s^{-2}$). Overlaid on the figure are sigma-t density contours.

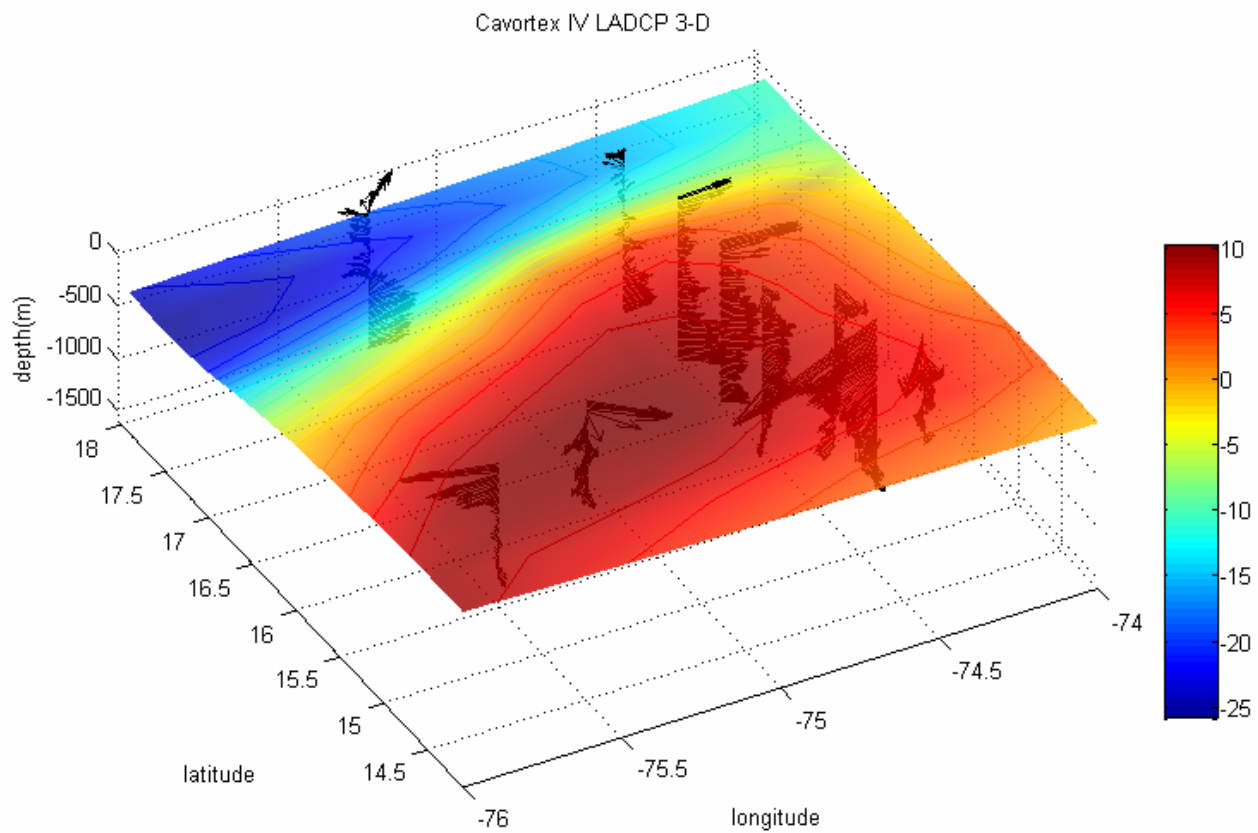


Figure 5.2.18 AVISO SSHA (cm) overlaid on LADCP velocity profiles. The largest arrow represents a velocity of 80 cm/s.

5.3 The cyclone-anticyclone eddy pair

The interaction of a cyclonic eddy with a small anticyclonic eddy was studied during Cavortex II from June 22-27, 2004 aboard the R/V Chapman. Satellite altimetry showed a large cyclone interacting with a small anticyclone about 100 miles south of Puerto Rico (*Figure 5.3.1*).

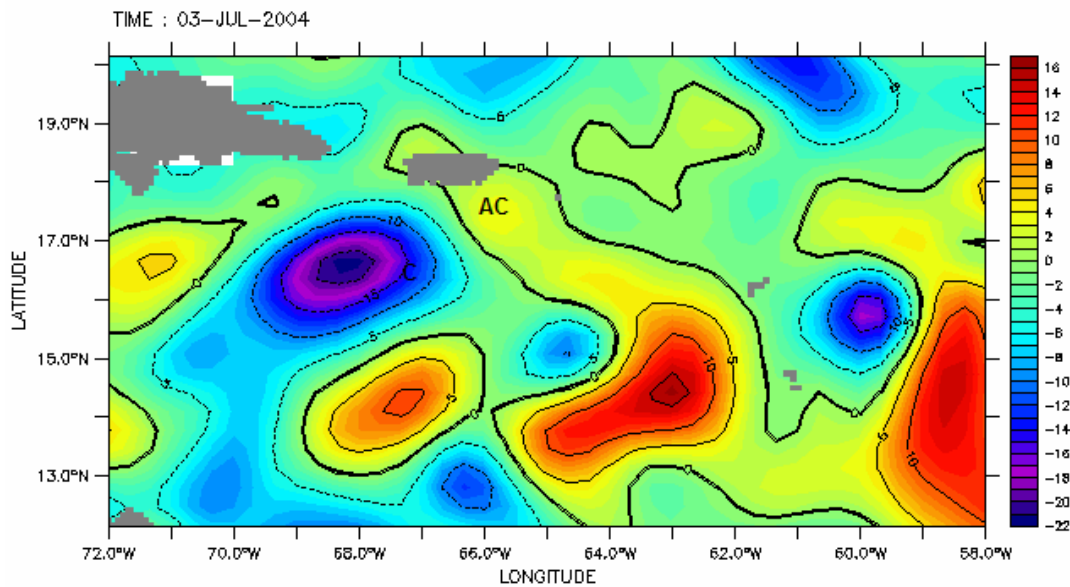


Figure 5.3.1 AVISO altimetry for July 03, 2004 shows the interaction between the cyclonic eddy (C) and a small anticyclonic eddy (AC).

Subsurface sampling confirmed the existence of both features as seen in the density structure, with the cyclone and anticyclone causing shoaling and deepening of isopycnals, respectively. The gradient from the negative SSHA to the positive SSHA was sampled in the survey. The notation used in the contour plots to represent the spatial scale of the eddy is the distance in kilometers from the each station to the first (*see Figure 5.3.2*). This was due to the diagonal nature of the cruise track.

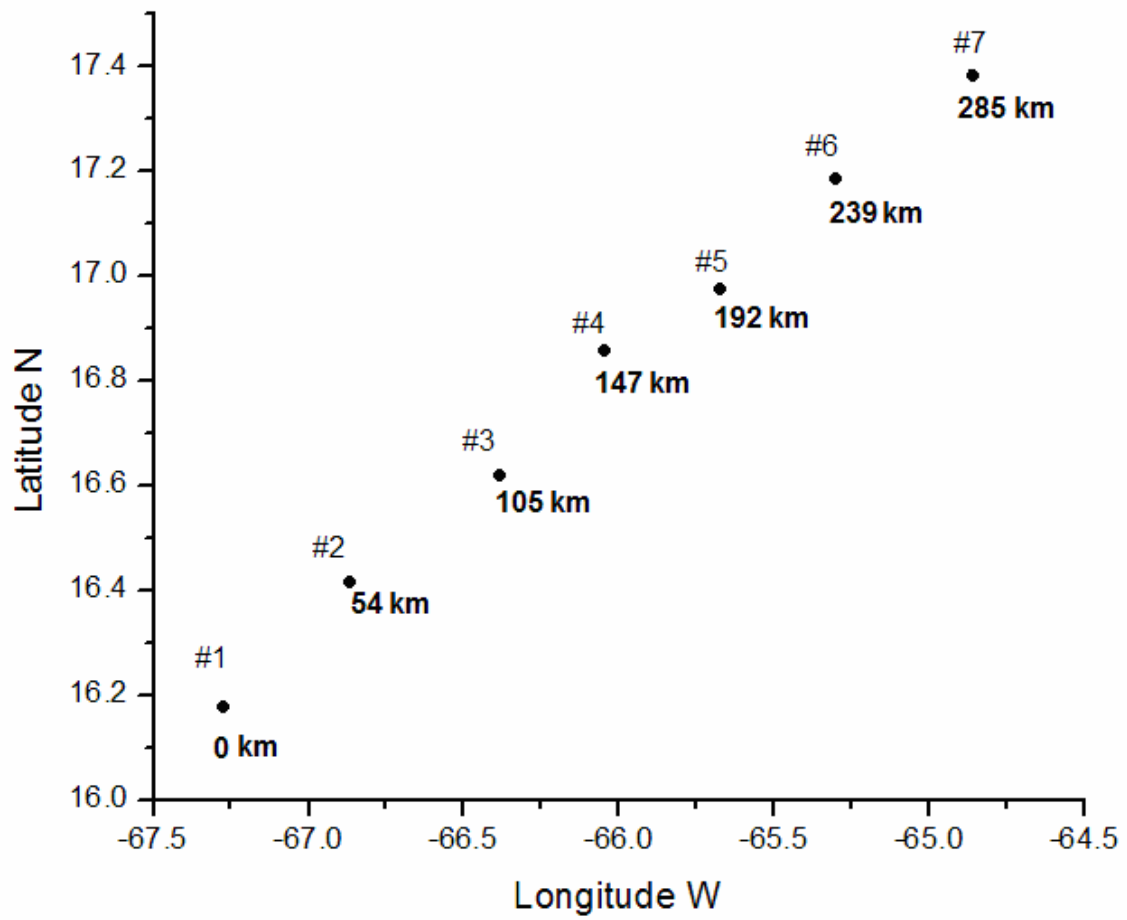


Figure 5.3.2 Notation used in the contour plots. Each black dot denotes a station, and the distance from each station to the first is given.

5.3.1 Formation, development and motion

Satellite altimetry reveals a small cyclone squeezing into the Caribbean Sea through or near the Anegada Passage (AP). On March 27, 2004 SSHA contours showed a small cyclone about 200 miles east of Puerto Rico. This eddy advected southwestward and by mid-April it appeared to be squeezing into the Caribbean through the AP, reaching inside the Caribbean by the end of April, when it was located ~150 miles southeast of Puerto Rico. The eddy merged with another small cyclone to its southeast and traveled westward. Meanwhile a small anticyclonic circulation with a weak SSHA signal appeared south of the AP. The origin of this structure is less clear, but by mid-June SSHA revealed an interaction between the two structures, forming an eddy pair (*Figure 5.3.3*). Even though the SSHA signal of the anticyclone was weak, LADCP profiles revealed velocities indicating anticyclonic circulation. This is the motivation to consider it a small anticyclonic eddy despite the absence of clearly defined closed streamlines in satellite data, as was a requirement when a mesoscale eddy was defined in the introduction of this study. The origin of these interacting structures appears to be closely related to the inflow of water and/or vorticity through the AP.

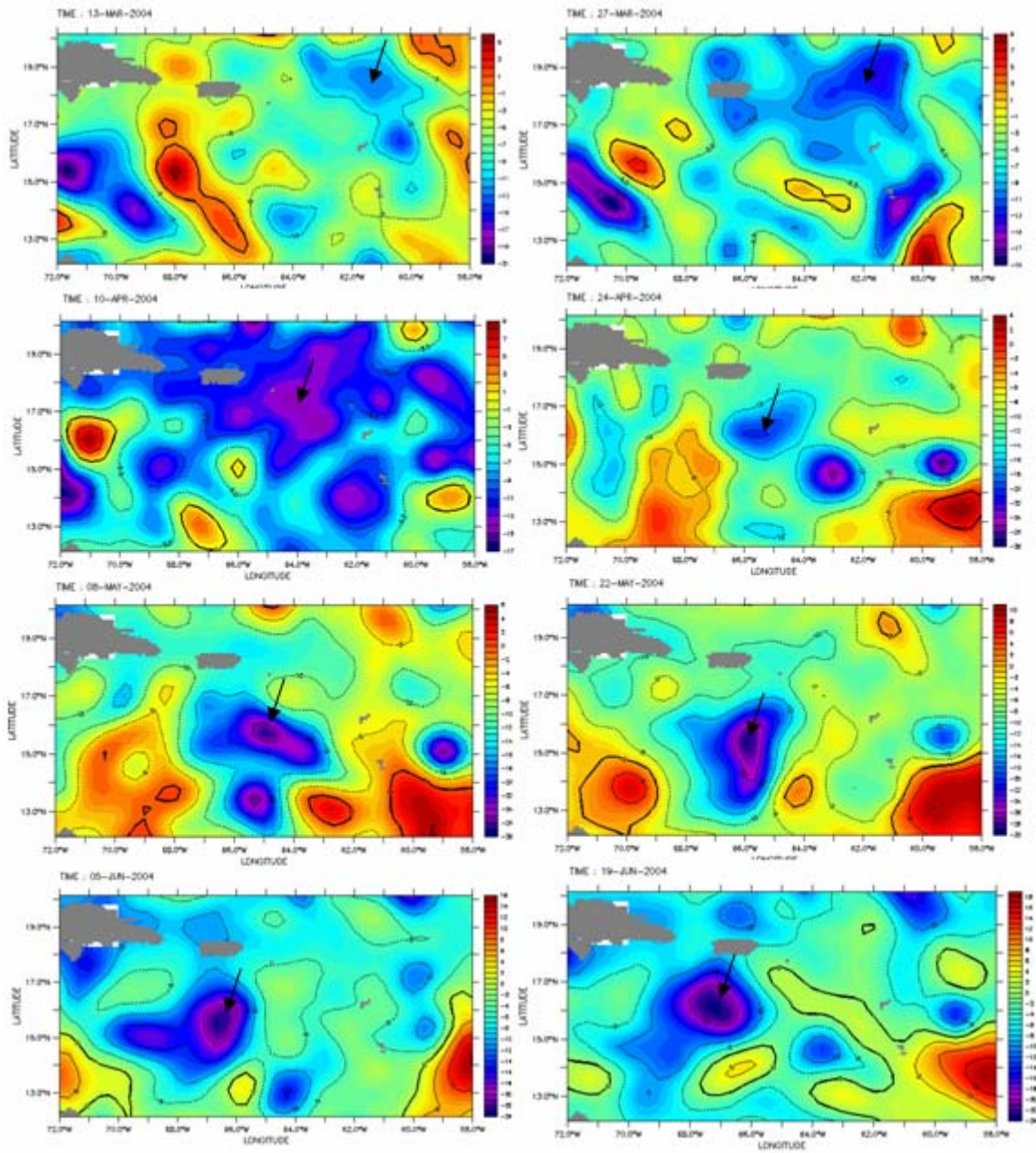


Figure 5.3.3 AVISO SSHA showing the origins of the interacting features. The arrow shows the location of the cyclonic eddy as it entered the Caribbean. The other component of the eddy pair, the small anticyclone, is seen to the right of the cyclone. Due to its weak SSHA signal, its origin is less clear.

5.3.2 Hydrography

The density structure obtained from CTD data shows shoaling of isopycnals due to the cyclone at depth 1000 meters or more. The cyclonic part of this pair seems to have a very deep reaching structure, possibly due to its origins near the Anegada Passage which has a sill depth of 1900 meters. The anticyclonic part; however, seems to have a shallower impact on the density structure, with deepening of isopycnals occurring no deeper than 400 meters. This may be due to the weak nature of this small eddy.

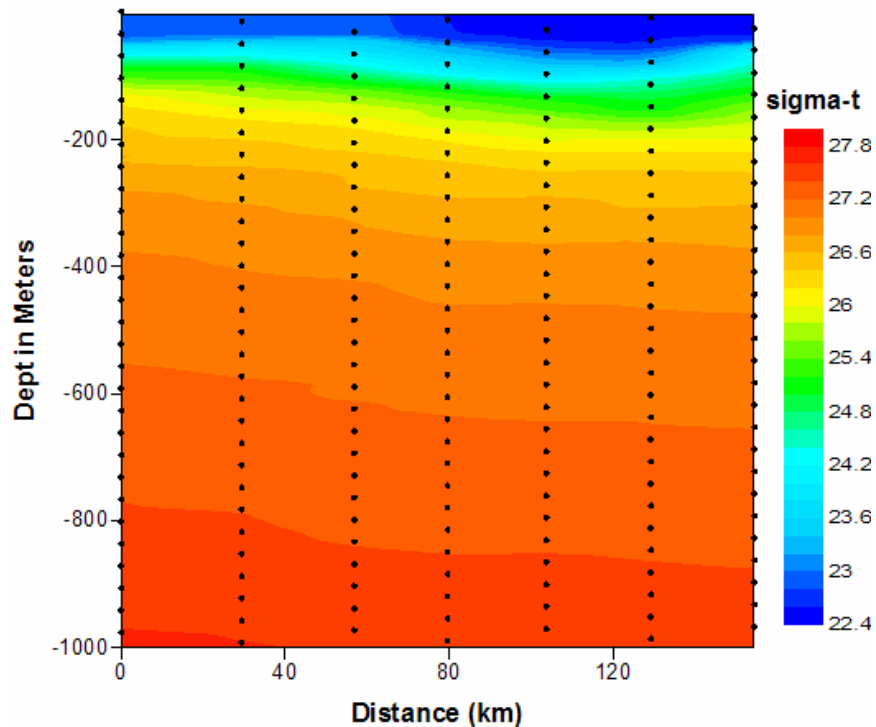


Figure 5.3.4 Density structure of the eddy pair shows shoaling of isopycnals to the left and deepening to the right caused by the cyclone and anticyclone, respectively.

High resolution Nu-Shuttle temperature data reveals the small-scale effects of the eddies on the thermal structure of the near surface layer (*Figure 5.3.5*). The cyclonic part shoals isotherms and creates a shallower mixed layer. It brings colder, nutrient rich water

into the euphotic zone, where phytoplankton can use the extra nutrients. The anticyclonic part creates deepening of isotherms and a deeper mixed layer.

The near surface salinity structure is also affected by the vertical displacements caused by the eddies (*Figure 5.3.6*). The cyclone creates shoaling of isohalines, bringing saltier water closer to the surface. The anticyclonic part creates deepening of isohalines, pushing fresher water to greater depths.

Temperature staircases were evident within the eddy pair, with the most pronounced structure found in the transition zone between the eddies (*Figure 5.3.7*).

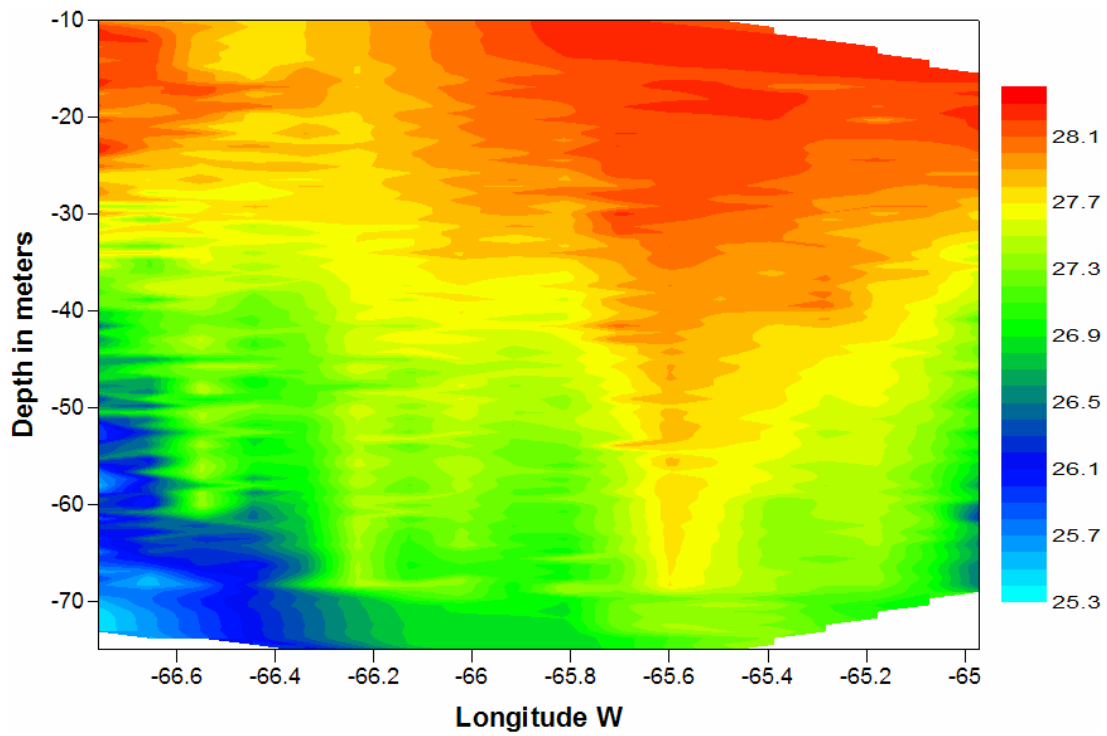


Figure 5.3.5 Nu-Shuttle temperature data shows the effects of the eddy in the near surface layer, causing changes in its thermal structure and in mixed layer depth.

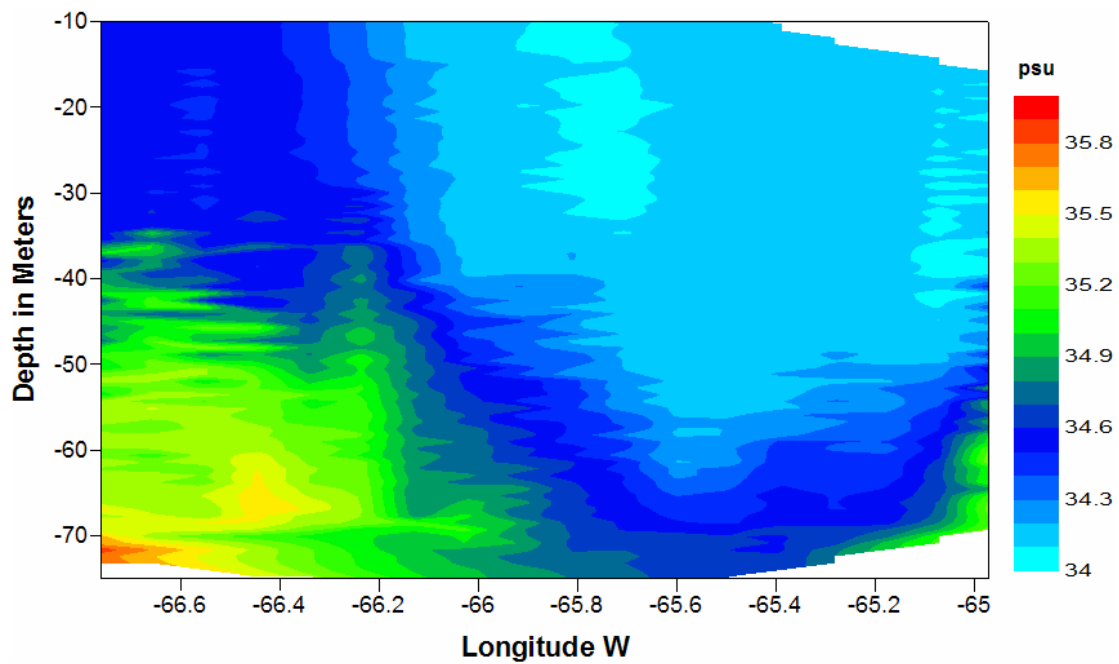


Figure 5.3.6 Nu-Shuttle salinity data shows displacement of isohalines in the near surface layer.

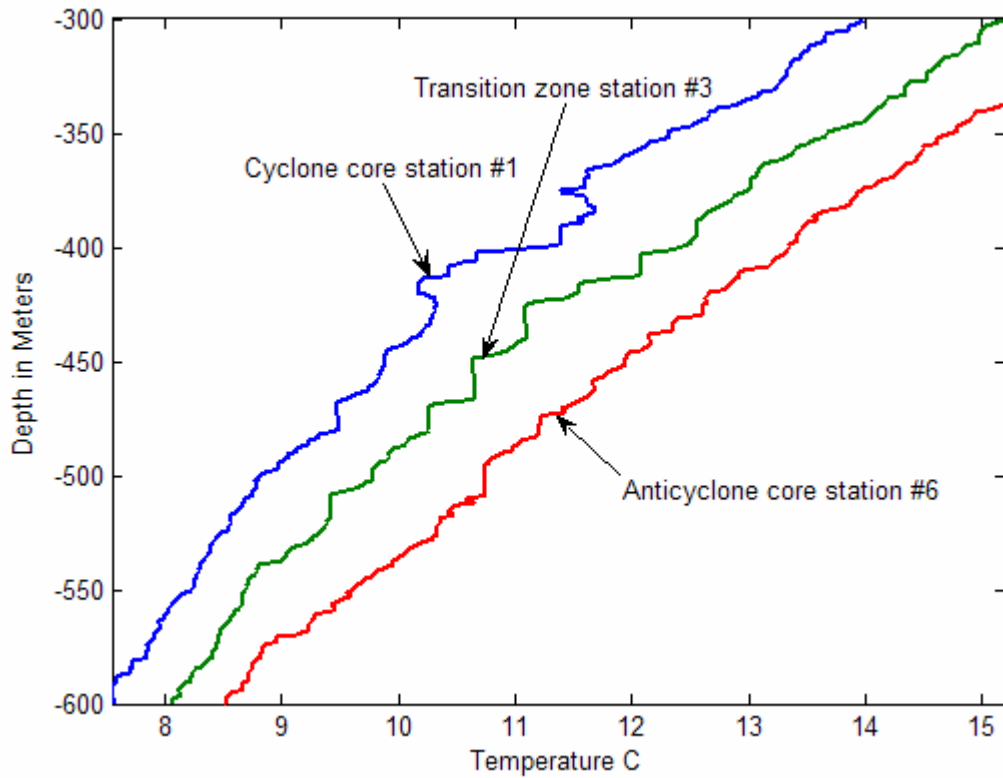


Figure 5.3.7 Temperature staircasing at different stations within the eddy pair. Staircases are more defined at the transition zone between the eddies than at their cores.

5.3.3 Velocity Structure

Both geostrophic and LADCP velocity measurements confirm the existence of the eddy pair. The calculated geostrophic velocity, with an assumed level of no motion at 1000 meters, shows maximum speeds of 55 cm/s and 15 cm/s for the cyclonic and anticyclonic parts, respectively (*Figure 5.3.7*). The small geostrophic velocity for the anticyclone is additional evidence of its weak nature.

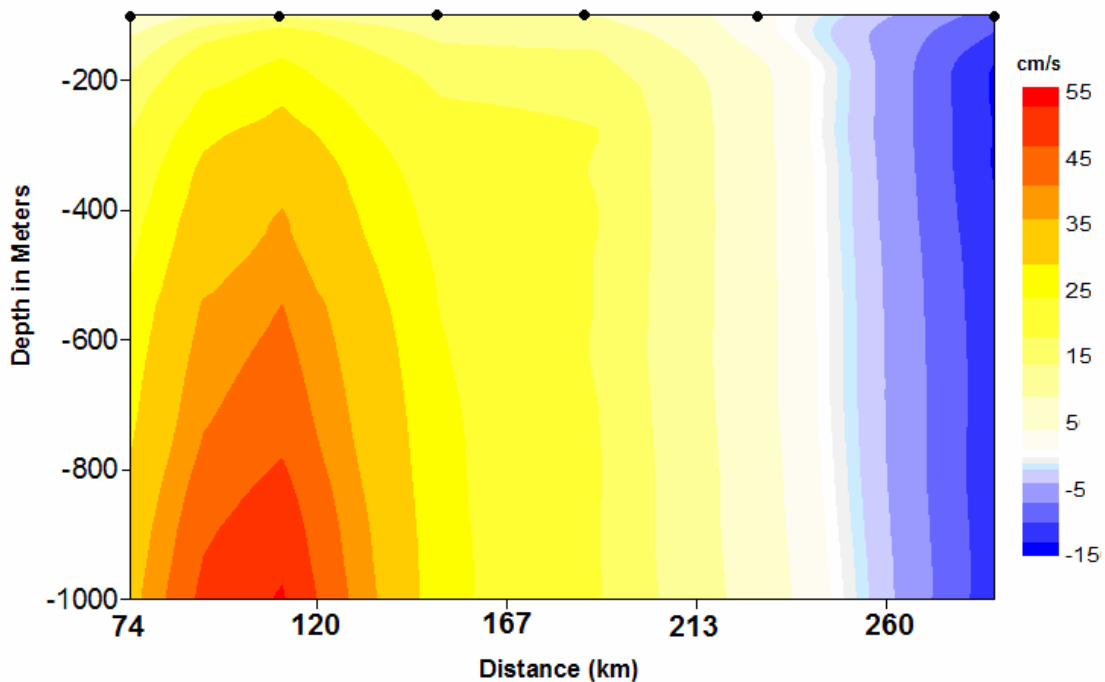


Figure 5.3.8 Contour plot of calculated geostrophic velocity in cm/s along the cruise track. Positive values indicate a flow into the figure, a northwesterly flow.

Direct measurements of the current velocity using an LADCP show similar circulation. The cyclonic part of the structure shows a deep reaching flow, and the first station shows a very barotropic profile (*Figures 5.3.8 & 5.3.9*). Overall the vertical current shear was weak, not reaching values greater than 10^{-5} s^{-2} (*Figure 5.3.10*) anywhere in the eddy pair.

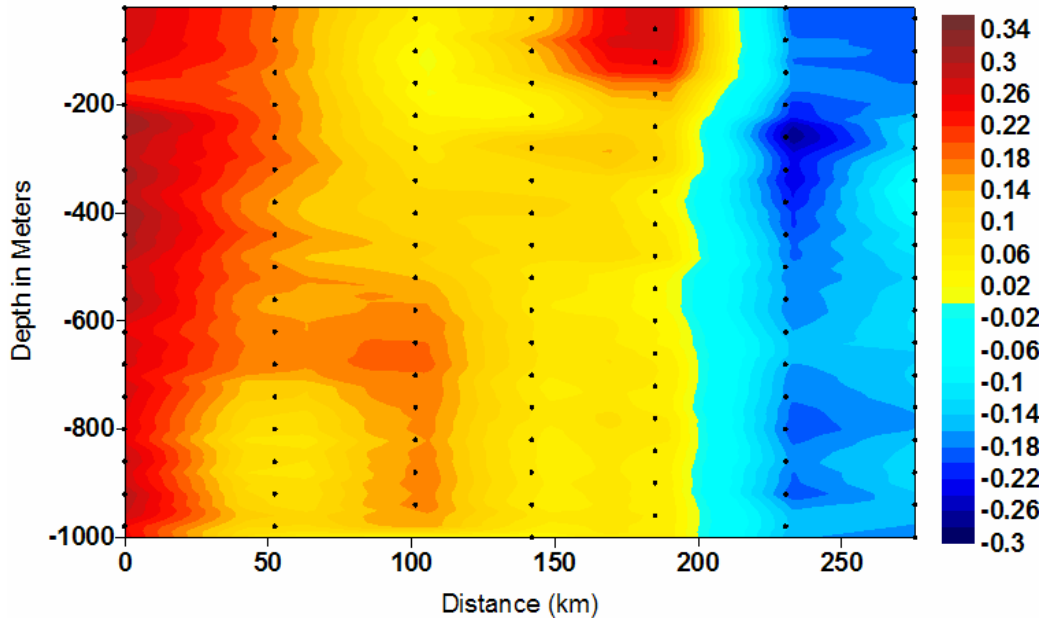


Figure 5.3.9 Contour plot of the meridional component of velocity in meters per second from LADCP data.

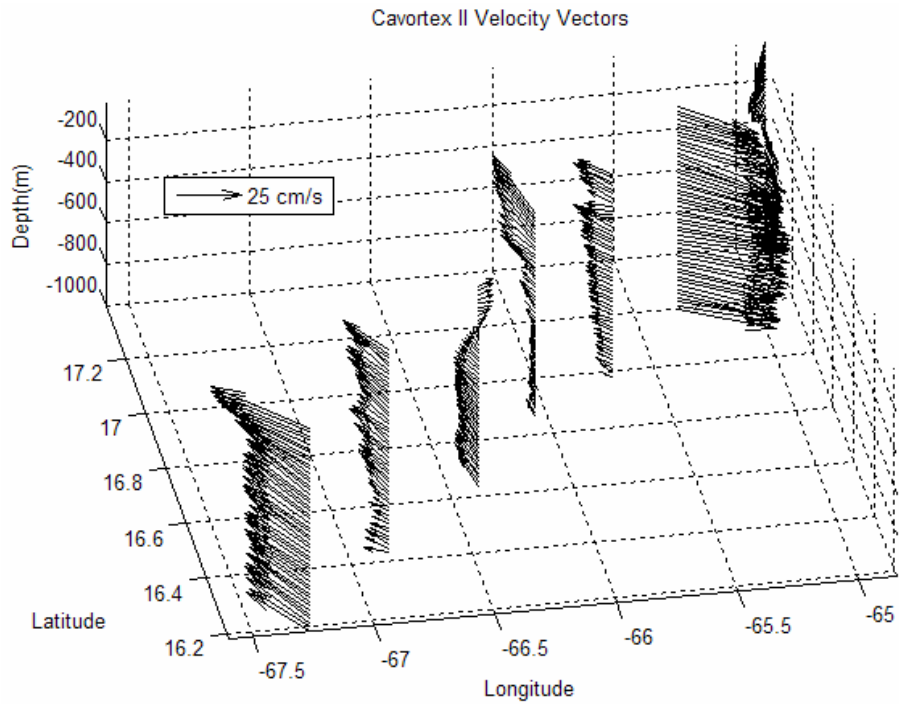


Figure 5.3.10 Quiver plot of the current velocity from LADCP profiles.

No large values of estimated diapycnal diffusivity were found except at single data points that may be outliers (*Figure 5.3.11*). Strong stratification and weak shear were responsible for this. However temperature staircasing was found, with the most pronounced structures found in the transition zone between the eddies. *Schmitt et al. (2005)* found that thermohaline staircases driven by salt fingers can significantly enhance diapycnal mixing.

The three-dimensional velocity structure of the eddy pair, with overlaid SSHA values is depicted on *Figure 5.3.12*. Note that the velocity vectors are nearly tangent to SSHA isolines, which in geostrophic theory would be streamlines.

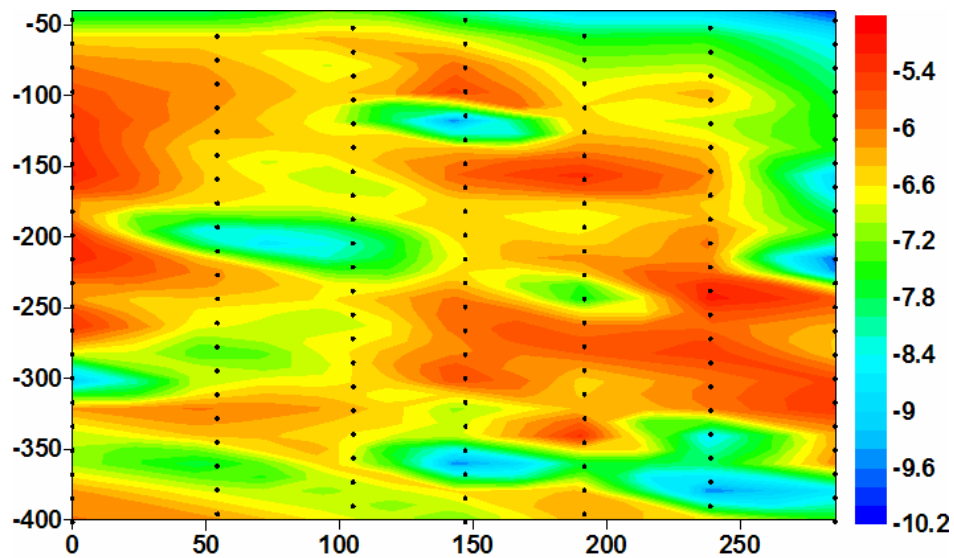


Figure 5.3.11 Contour plot of the base 10 logarithm of LADCP current shear squared (in s^{-2}).

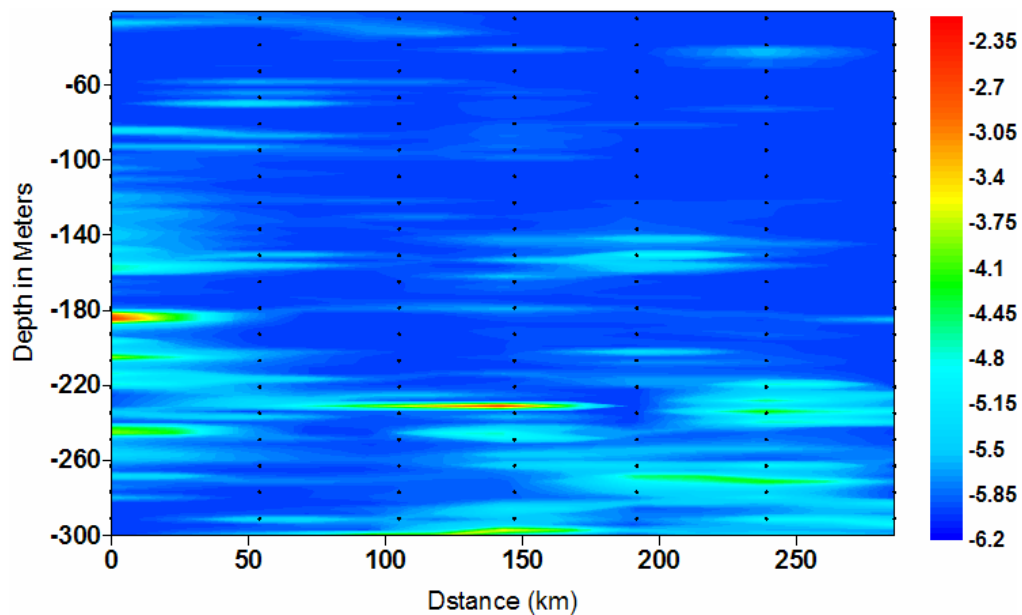


Figure 5.3.12 Transect of estimated \log_{10} diapycnal diffusivity (in $m^2 s^{-2}$), black dots denote individual stations. Besides some isolated “hot spots”, there is no evidence to indicate enhanced diffusivity within the structure.

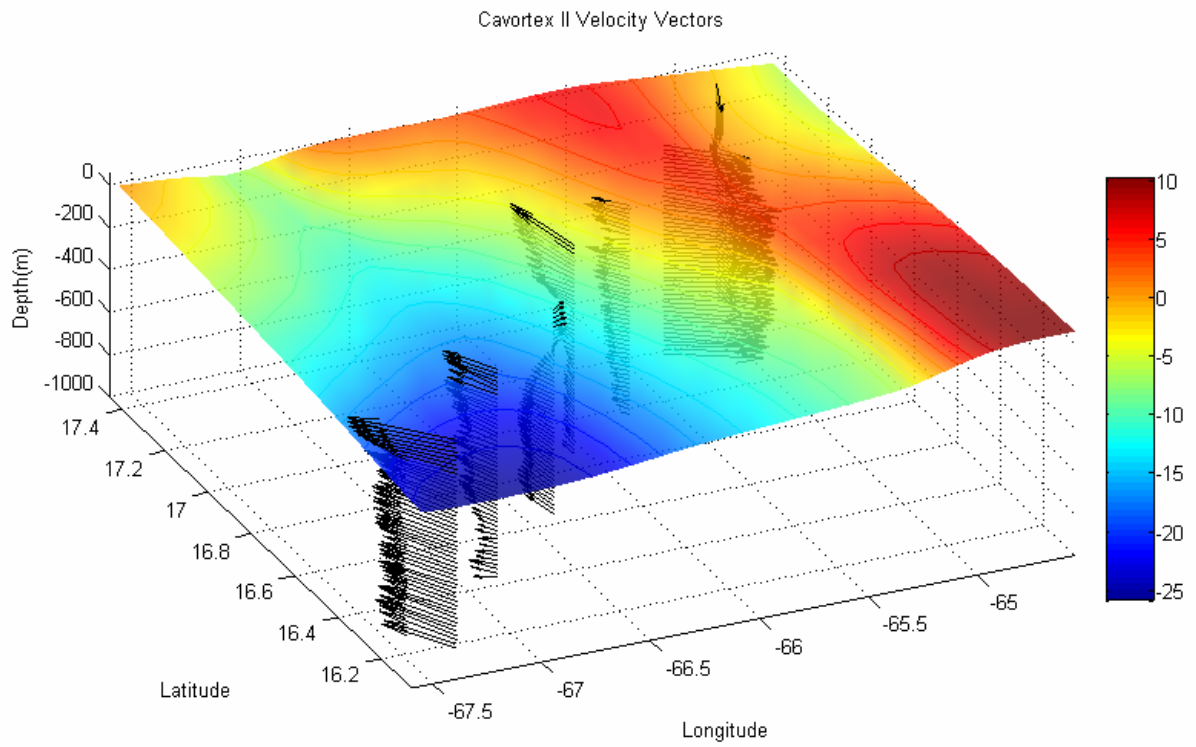


Figure 5.3.13 AVISO merged SSHA (cm) overlaid on LADCP velocity profiles. The largest arrow represents a velocity of 55 cm/s.

5.4 Comparing the three features

Besides the obvious difference in sense of rotation there is substantial variability between the features. Differences are evident in their formation and path into the Caribbean, their velocity and hydrography. *Table 5.1* summarizes some descriptive characteristics of the features at the time they were surveyed.

			<i>Eddy Pair</i>	
	<i>Cyclone</i>	<i>Anticyclone</i>	<i>Cyclone</i>	<i>Small Anticyclone</i>
Radius (average)³	~100 km	~150 km	~140 km	~25 km
Maximum geostrophic swirl velocity (baroclinic component)	~40 cm/s	~35 cm/s	~50 cm/s	~15 cm/s
Maximum LADCP swirl velocity	N/A ⁴	~60 cm/s	~60 cm/s	~40 cm/s
Propagation⁵ velocity	9 cm/s	12 cm/s	7 cm/s	6.5 cm/s
Vertical extent of isopycnal displacement⁶	~700 m	>1000 m	>1000 m	~400 m
Maximum SSHA signal (AVISO)	-8 cm	+12 cm	-24 cm	+4 cm
Depth of the 26 sigma-t isopycnal at maximum displacement	143 m	230 m	127 m	199 m
Coordinates of eddy “center”⁷	14.9 N 67.4 W	15.2 N 75.3 W	16.5 N 68.0 W	17.5N 65.7 W (center not clearly defined)
Rossby number $Ro = \frac{U}{fL}$	0.11	0.07	0.08	0.4

Table 5.1 Some descriptive characteristics of the features at the time they were surveyed.

³ Given the asymmetric nature of some features, this is the average of the radius to the N, S, E and W of the center.

⁴ An LADCP was not available for this cruise.

⁵ Each feature was tracked using SSHA maps and the velocity represents a 1 month average before and during the cruise dates.

⁶ Represents the deepest part of the water column that presented isopycnal displacements, deepening in anticyclones and shoaling in cyclones.

⁷ Refers to the approximate position inferred from SSHA maps for the date of the cruise.

5.4.1 Formation, development and motion

The early stages of the three features seem to have entered the Caribbean Sea as vorticity advected thru passages. They then intensified once inside the Caribbean. Both the anticyclone and the eddy-pair seem to have made their way inside through or near the Anegada Passage. The cyclone however first appeared inside the Caribbean near the St. Vincent Passage. The strengthening of the cyclone appeared to be catalyzed by the cyclonic shear to the west of the anticyclone that was impinging on the Lesser Antilles. But the strengthening of the other features is less clear. SSHA plots imply that the cyclonic part of the eddy pair intensified after merging with two other lesser cyclones. The anticyclonic part of the eddy pair did not intensify at all and months later seems to have been absorbed by a larger anticyclone to its south.

Prior to merging with another anticyclone by late March, the anticyclone surveyed near Jamaica advected westward through the Caribbean for six months, undergoing periods of intensification and weakening as implied by its SSHA signal that are not easily explained. The approximate trajectories of the features from their appearance inside the Caribbean until the time they were surveyed are depicted in *Figure 5.4.1*.

A notable fact is the difference in sill depth of the passage through which their vorticity was advected. For the anticyclone and the eddy pair this depth is 1900 meters, while for the cyclone it is 800 meters. The possible effects of this difference on the vertical structure of the eddies is addressed in the next section.

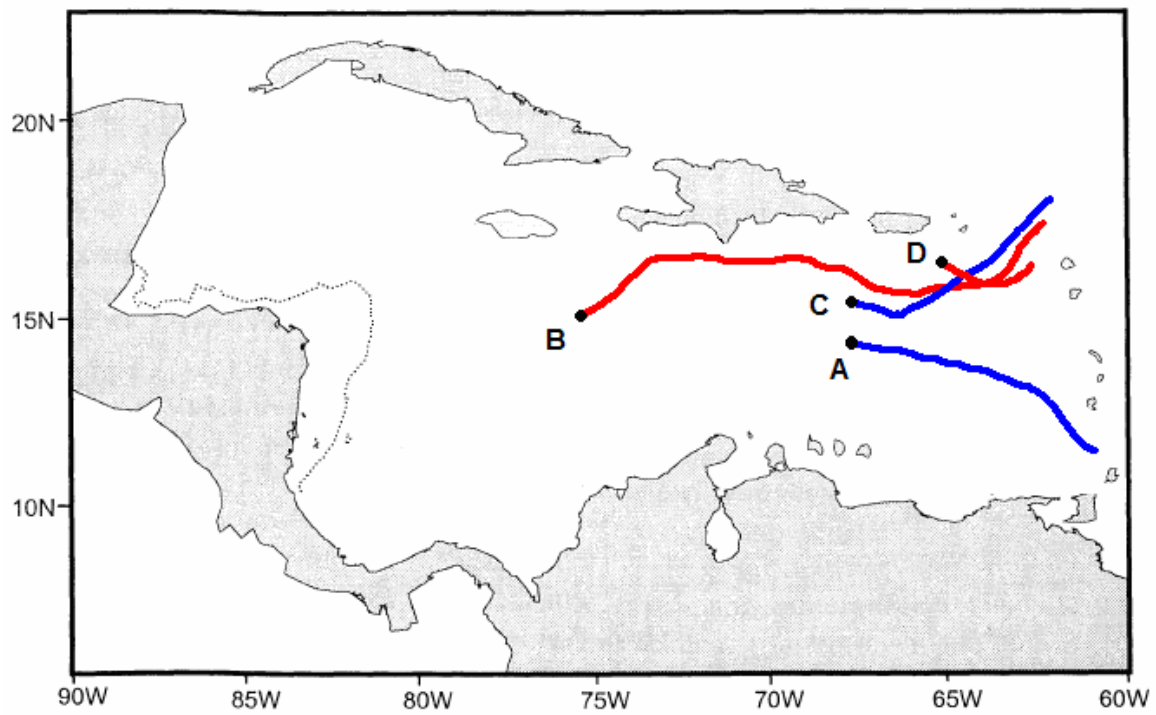


Figure 5.4.1 Approximate trajectories inferred from SSHA plots of the cyclone (A), the anticyclone (B) and the cyclone (C)-anticyclone (D) eddy pair. The black dot marks the approximate position of the eddy at the time of each cruise.

5.4.2 Hydrography

The vertical extent of the impact of the eddies on the density structure of the water column was different for each. The cyclone only appeared to reach 700 meters, while the impact of the anticyclone was visible at depth greater than 1000 meters. The cyclonic part of the eddy pair also reached more than 1000 meters, while the anticyclonic part only seemed to affect the upper 400 meters of the water column. The cyclone was the only structure of the eddies studied that presented significant advection of ORP water, evident in both the shallow salinity and density structure.

Analysis of the temperature-salinity relationship for each feature revealed variability in both the shape and in the tightness of the curves (*Figure 5.4.2*). The anticyclone and the eddy pair share a very similar Temperature-Salinity (T-S) relationship for water colder than 23 degrees Celsius. This is particularly interesting given the fact that they were sampled more than a thousand kilometers apart. This similarity seems to be explained by the fact that both features made their way into the Caribbean through the Anegada Passage (AP). With sill depths of 1900 meters, the AP contributes about 2.5 Sv of transport into the Caribbean (*Johns et al., 2002*). These eddies may play an important role in modulating this transport.

The cyclone's T-S relationship deviated significantly from that of the other two structures. For water warmer than seven degrees Celsius, the relationship was especially different. This may be due to the difference in the origins of this eddy. This structure appears to have intensified due to the impingement of an anticyclone, possibly a NBCR, into the Lesser Antilles. The cyclone first appeared near the St. Vincent passage which has a sill depth of about 800 meters. This may account for its limited vertical extent and

different T-S relationship. There is also a presence of warm, low salinity water that corresponds to the ORP water being advected by the eddy.

The differences in the T-S relationship between structures merit a detailed water mass structure analysis. However, it is outside the scope of the present study.

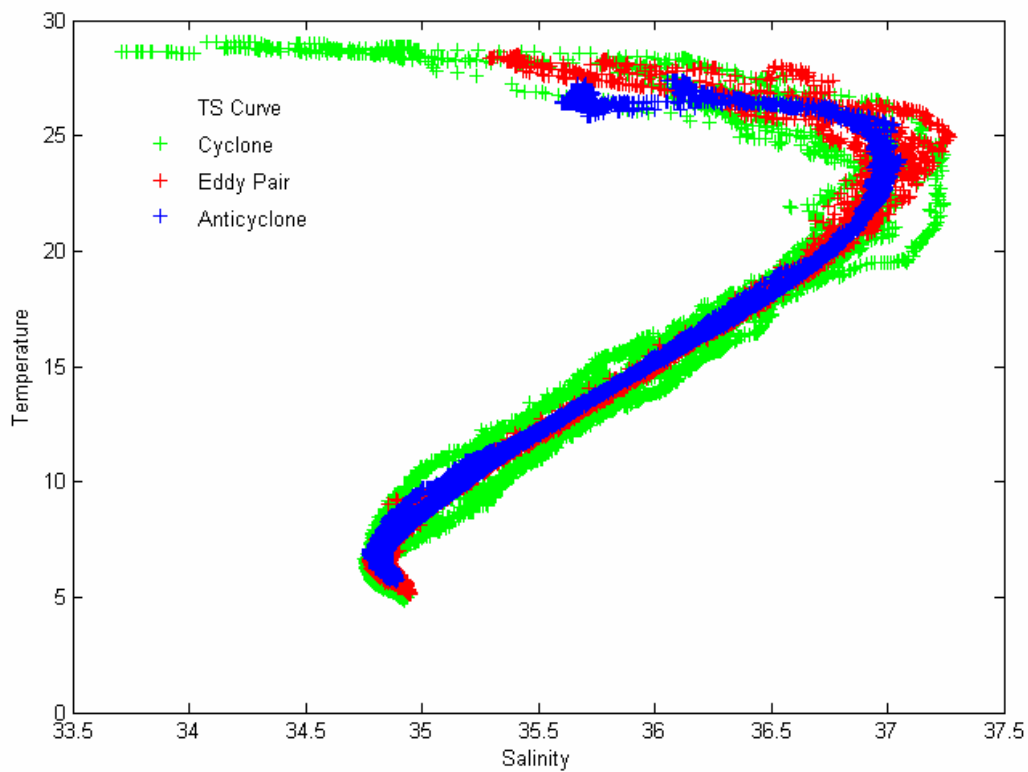


Figure 5.4.2 Temperature-Salinity relationship for the three features: the cyclone, the anticyclone and the eddy pair. The data represent all CTD stations from each cruise.

There is a positive relationship in all of the eddies between their maximum SSHA and their isopycnal depths. This relationship is shown on *Figure 5.4.3* for the 25 & 26 sigma-t isopycnals. For these specific isopycnals, if a linear relationship is assumed, there is a slope of a ~ 3 meters of isopycnal displacement per 1 cm of SSHA. However a linear relationship is very unlikely. Previous studies on mesoscale eddies in the Bermuda Atlantic Time Series (BATS) have revealed a slope of 4 meters per 1 cm of SLA (*McGillicuddy et al., 1998*).

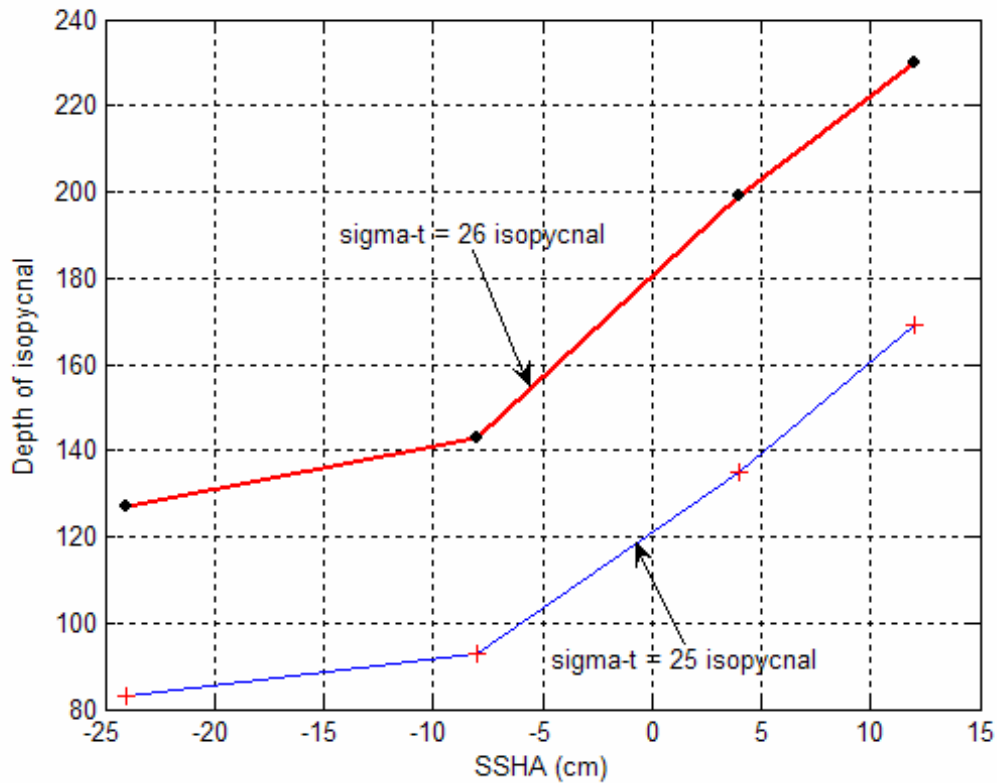


Figure 5.4.3 Depth of the 25 & 26 sigma-t isopycnals at maximum displacement compared with the SSHA of each feature at its center.

Thermohaline staircases

There seems to be a trend in the spatial distribution of thermohaline staircases within the eddies. The most intense and better defined staircases were found in the edges of the eddies for all the features in this study. At their cores, eddies presented staircases that were much less defined than the ones found in the edges. The cyclonic part of the eddy pair did show some staircasing, but not as dramatic as in the transition zone.

The formation of staircases has been related to the phenomenon of salt fingers. Salt fingers are formed due to the larger molecular diffusivity of temperature as compared to salinity. This leads to preferential mixing of heat over salt within the water column when warmer saltier water is located above colder, fresher water. This is the process known as differential diffusion. For a review see *Gargett (2001)*.

The distribution of the better defined staircases suggests that in the eddy cores, thermohaline staircases are less abundant. However not all stations at the eddy edges showed well defined staircases. The mechanism that leads to better defined and more abundant staircasing in the eddy edges is a mystery. It is unclear whether the staircasing is formed in the eddy edges or if previously existing staircases were dissipated by the isopycnal shoaling that occurs at a maximum in the core of an eddy.

5.4.3 Velocity structure

The velocity structure of the cyclone cannot be directly compared to that of the anticyclone and the eddy pair due to the absence of LADCP data. Given the uncertainties due to the assumption of the level of no motion, the geostrophic velocity will not be used to compare the features.

The anticyclone presented a surface intensified velocity structure but it still presented coherent anticyclonic circulation deeper than 1000 meters. The cyclonic part of the eddy pair also showed circulation as deep as 1000 meters, but its velocity profile was more barotropic. The anticyclonic part of the eddy pair also showed circulation as deep as 1000 meters. The anticyclone presented stronger shear, which caused in part the larger values of diapycnal diffusivities found in this structure. It is unclear whether the differences in velocity structure were caused by the merging that the anticyclone was undergoing at the time of the survey.

Diapycnal mixing:

Because of the unavailability of direct velocity measurements during the survey of the cyclone, vertical mixing coefficients were not calculated for this structure. For both the anticyclone and the eddy pair estimates were made based on the *Pacanowski and Philander (1981)* mixing scheme. Average values for both features were about $10^{-5.5} \text{ m}^2 \text{ s}^{-1}$. These are smaller values than have been reported in the Caribbean Sea by Morell et al. (2001) using a different parameterization, which were on the order of $10^{-3} \text{ m}^2 \text{ s}^{-1}$. It is unclear whether this disagreement is due to the difference in methodology or due to ambient conditions. Only the anticyclone presented an area of significant enhancement

of estimated diapycnal mixing in its southern edge. This was due to a combination of increased shear and a decrease in stratification.

Thermohaline staircasing has been recently shown to enhance diapycnal mixing in the Tropical Atlantic (Schmitt et al., 2005). They found average thermocline diffusivities of $0.9 * 10^{-4} \text{ m}^2\text{s}^{-1}$ using direct observations from tracer release experiments. These values are greater than what would have been estimated using a parameterization based on mechanical turbulence (Schmitt et al., 2005) such as Pacanowski and Philander (1981).

The increase in thermohaline staircasing found in this study in the edges of the eddies may be responsible for greater diapycnal diffusivities than were estimated using a mechanical turbulence based parameterization. Indeed the clue to the “missing mixing” question that arises when the results of this study are compared with previous literature may lie on this process, which is unresolved by the Pacanowski and Philander (1981) mixing scheme. Much more detailed studies are needed to reconcile diapycnal mixing estimates in the Caribbean and the Tropical Atlantic.

6. Conclusions

The three-dimensional structure of three mesoscale features: a cyclone, an anticyclone and an eddy pair have been described based on their hydrography and velocity structure. Using SSHA plots, their movement and possible formation mechanisms were inferred. The main conclusions are the following:

1. Mesoscale eddies in the Caribbean are highly variable features both in their three-dimensional structure and in their origins.
2. For the features studied, vorticity advected through passages seems to have been their formation and/or strengthening mechanism.
3. The vertical extent of their impact on the density structure of the water column may be related to the sill depth of the passage where their vorticity was advected into the Caribbean.
4. Once inside the Caribbean these features strengthen considerably and merge with other eddies while being advected by the mean flow.
5. Maximum swirl speeds ranged from 30-60 cm/s and their propagation speeds were 6-12 cm/s.
6. Of the two features sampled directly with an LADCP, both had a coherent velocity structure that extended deeper than 1000 meters.
7. In the Caribbean Sea, assuming a level of no motion of 1000 meters when calculating geostrophic velocity is a questionable assumption.
8. Thermohaline staircases are better defined and more abundant in the eddy edges, and may contribute to enhanced diapycnal mixing in these areas.

Perhaps more importantly, this research has posed several questions that remain unanswered:

1. Why are thermohaline staircases more prevalent in the eddy edges than in their cores?
2. How deep can the velocity structure of Caribbean mesoscale eddies reach?
3. What is the role of these mesoscale eddies in the vertical mixing of water masses?
4. What mechanisms are responsible for the strengthening and/or weakening of these eddies as they propagate across the Caribbean?

In conclusion, although some evidence is presented towards its acceptance, more detailed studies are needed to formally confirm or reject the hypothesis formulated earlier in this study, that the three-dimensional structure of the eddies will vary depending on their formation mechanism and/or their path into the Caribbean Sea.

7. References

- Alfonso, E. 2001. Ph.D. Thesis. University of Puerto Rico.
- Beckmann, A. 1988. Vertical structure of midlatitude mesoscale instabilities. *J. Phys. Oceanography*, 18, 1354–1371.
- Bracco A. , A Provenzale and I. Scheuring. Mesoscale vortices and the Paradox of the Plankton. (2000). *Proc. R. Soc. Lond.* 267, 1795-1800
- Corredor et. al. (2004) Cyclonic Eddy Entrains Orinoco River Plume in Eastern Caribbean. *EOS* , Vol. 85, No. 20, 18 May 2004, pages 197, 201-202.
- Firing, E., Lowered ADCP and use in WOCE. *International WOCE Newsletter*. p 10-15, 1998
- Firing, E., and R. Gordon, Deep ocean acoustic Doppler current profiling, in *Proceedings of the IEEE Fourth Working Conference on Current Measurements*, April 3-5, Clinton, Maryland, pp. 192-201, 1990.
- Fischer, J., and M. Visbeck, Deep velocity profiling with self-contained ADCPs., *J. Atmos. Oceanic Technol.*, 10 , 764-773, 1993.
- Fratantoni, D.M., and Glickson, D.A. (2002) North Brazil Current Ring Generation and Evolution Observed with SeaWiFS. *Journal of Physical Oceanography*. 32, 1058-1074.
- Fuglister, F.C., 1951. Annual variations in current speeds in the Gulf Stream System. *Journal of Marine Research*, 10, 119–127.
- Gargett, A. E. 2001. Differential diffusion: an oceanographic primer. *Progress in Oceanography*, 56 (3-4), 559-570.
- Gill, A. E., J. S. A. Green, and A. J. Simmons, 1974. Energy partition in the large-scale ocean circulation and the production of midocean eddies. *Deep-Sea Res.*, 21, 499–528.
- Goni, G.J. and Johns, W.E., 2003. Synoptic study of warm rings in the North Brazil Current retroflection region using satellite altimetry. In: Goni, G.J., Malanotte-Rizzoli, P. (Eds.), *Interhemispheric Water Exchange in the Atlantic Ocean*. Elsevier Oceanographic Series 68, Elsevier, Amsterdam, pp. 335–356.
- Heburn, G.W., T. Kinder, J. Allender and H. Hurlburt, A numerical model of eddy generation in the southeastern Caribbean Sea, in *Hydrographics of Semi-enclosed Seas*, edited by J. Nihoul, pp 299-328, Elsevier Sci., New york, 1982
- Johns, W.E., Townsend, T.L., Fratantoni, D.M., Wilson, W.D., 2002. On the Atlantic inflow to the Caribbean Sea. *Deep-Sea Research I*, 49, 211–243.

Kinder, T.H., Shallow currents in the Caribbean Sea and the Gulf of Mexico as observed with satellite tracked drifters, *Bull. Mar. Sci.*, 33, 239-246, 1983.

Ledwell, J.R., A.J. Watson and C.S. Law. (1993). Evidence for slow mixing across the pycnocline from an open ocean tracer release experiment, *Nature*, 364, 701-703.

Lee, M. M. and R.G. Williams (2000). The role of eddies in the isopycnic transfer of nutrients and their impact of biological production. *Journal of Marine Research*, 58, pp. 895-917.

Logerwell E.A. and P. E. Smith (2001). Mesoscale eddies and survival of late stage Pacific sardine (*Sardinops sagax*) larvae. *Fisheries Oceanography*, Vol 10, Issue 1, 13.

Martin, A. P., K. J. Richards (1999). Mechanisms for vertical nutrient transport within a North Atlantic mesoscale eddy. *Deep Sea Research II*, 48, 757-773

McGillicuddy, D.J., et. al. (1998). Influence of mesoscale eddies on new production in the Sargasso Sea. *Nature*. 394: pages 263-266.

McNeil et al., 1999. New chemical, bio-optical and physical observations of upper ocean response to the passage of a mesoscale eddy off Bermuda, *Journal of Geophysical Research*, Vol. 104, C7, pp 15,537–15,548

Miles, J.W., (1961) On the stability of heterogeneous shear flows, *Journal of Fluid Mechanics*, 10, pp 496-508.

Molinari, R.L., Atwood, D.K., Duckett, C., Spillane, M., Brooks, I., 1980. Surface currents in the Caribbean Sea as deduced from satellite tracked drifting buoys. *Proceedings of the Gulf and Caribbean Fisheries Institute*, 31, 106–115.

Morell, J.M., Capella, J., Mercado, A., Bauza, J., and Corredor J.E. (2001) Nitrous oxide fluxes in Caribbean and Tropical Atlantic waters: evidence for near surface production. *Marine Chemistry* 74:131-143.

Munk W. H., Abyssal Recipes, *Deep-Sea Res.*, 13, 207-230, 1966

Nyusten, J.A. and C.A. Andrade, Tracking mesoscale ocean features in the Caribbean Sea using Geosat altimetry, *J. Geophys. Res.*, 98, 8389-8394, 1993.

Murphy, S.J., H.E. Hurlburt, and J.J. O'Brien, The connectivity of eddy variability in the Caribbean Sea, the Gulf of Mexico and the Atlantic Ocean, *J. Geophys. Res.*, 104, 1431-1453, 1999.

Pacanowski, R.C. and S.G.H. Philander (1981). Parameterization of vertical mixing in numerical models of tropical oceans. *Journal of Physical Oceanography*. Vol. 11 No.11, pages 1443-1451.

- Pedlosky, J. (1979) *Geophysical Fluid Dynamics*. Springer-Verlag, N.Y., 728 pp.
- Proudman, J., (1953) *Dynamical Oceanography*. Methuen, London and John Wiley, N.Y., 409 pp.
- Ring Group 1981. Gulf Stream cold core rings: their physics, chemistry and biology. *Science* 212, 1091-1100.
- Sastre, M. (1999), M.S. Thesis. University of Puerto Rico.
- Schmitt, R.W., Ledwell J.R., Montgomery E. T., Polzin K. L. and Toole, J. M. 2005. Enhanced Diapycnal Mixing by Salt Fingers in the Thermocline of the Tropical Atlantic. *Science*, 38, pp. 685-699.
- Siegel, D.A., McGillicuddy, D., Fields, E.A. (1999) Mesoscale eddies, satellite altimetry and new production in the Sargasso Sea. *Journal of Geophysical Research*. Vol 104, pp 13,359-13,379.
- Simmons, H.L. and Nof, D. (2002). The squeezing of eddies through gaps. *Journal of Physical Oceanography*. 32, pp 314-335.
- Visbeck M. Deep Velocity Profiling using Lowered Acoustic Doppler Current Profiler: Bottom Track and Inverse Solutions. Submitted to *J. Atmos. Ocean Tech.*

Appendix I: Symbols and Notation

ρ = density

ρ_0 = reference density

ρ_θ = potential density

N = Brunt-Vaisala or stratification frequency

g = gravity = 9.8 m/s²

ν = kinematic viscosity

Ω = angular velocity of Earth = 7.29 x 10⁻⁵

u = velocity component in x direction

v = velocity component in y direction

w = velocity component in z direction

x = east

y = north

z = up (parallel to gravity vector)

ϕ = latitude

f = Coriolis parameter = $2 \Omega \sin \phi$; planetary vorticity

t = time

H = water column depth or layer thickness

T = water temperature

θ = potential temperature

α = specific volume of seawater

β = meridional gradient of the Coriolis parameter

ζ = relative vorticity

κ_d = vertical eddy diffusivity coefficient

O = on the order of

Acronyms:

OGCM = Ocean General Circulation Model

NBC = North Brazil Current

NBCR = North Brazil Current ring

CEs = Caribbean Eddies

WBC = Western boundary Current

LADCP = Lowered Acoustic Doppler Current Profiler

MOC = Meridional Overturning Circulation

AP = Anegada Passage

ORP = Orinoco River Plume